Systematic SO(10) operator analysis for fermion masses

G. Anderson*
Department of Physics, The Ohio State University, Columbus, Ohio 43210
S. Dimopoulos
Department of Physics, Stanford University, Stanford, California 94305
L. J. Hall
Department of Physics, University of California, Berkeley, California 94720
and Theoretical Physics Group, Physics Division, Lawrence Berkeley Laboratory, 1 Cyclotron Road, Berkeley, California 94720
S. Raby†
Department of Physics, The Ohio State University, Columbus, Ohio 43210
G. D. Starkman
Canadian Institute for Theoretical Astrophysics, University of Toronto, 60 George St., Toronto, Ontario M5S 1A7, Canada
(Received 27 August 1993)

A new approach for deducing the theory of fermion masses at the scale of grand unification is proposed. Combining SO(10) grand unification, family symmetries and supersymmetry with a systematic operator analysis, the minimal set of fermion mass operators consistent with low-energy data is determined. Exploiting the full power of SO(10) to relate up, down, and charged lepton mass matrices, we obtain predictions for seven of the mass and mixing parameters. The assumptions upon which the operator search and resulting predictions are based are stressed, together with a discussion of how the predictions are affected by a relaxation of some of the assumptions. The masses of the heaviest generation, m_t, m_b, and m_τ, are generated from a single renormalizable Yukawa interaction, while the lighter masses and the mixing angles are generated by nonrenormalizable operators of the grand unified theory. The hierarchy of masses and mixing angles is thereby related to the ratio of grand to Planck scales, M_G/M_P. An explicit realization of the origin of such an economical pattern of operators is given in terms of a set of spontaneously broken family symmetries. In the preferred models the top quark is found to be heavy, $M_t = 180 \pm 15$ GeV, and $\tan\beta$ is predicted to be very large. Predictions are also given for m_s, m_s/m_d, m_u/m_d, V_{cb}, V_{ub}/V_{cb} and the amount of CP violation. Stringent tests of these theories will be achieved by more precise measurements of M_t, V_{cb}, α_s, and V_{ub}/V_{cb} and by measurements of CP violation in neutral B meson decays.

PACS number(s): 12.15.Ff, 12.15.Hh, 12.60.Jv

I. INTRODUCTION

The standard model is unlikely to be a fundamental theory: it contains 19 parameters, 13 of which belong to the flavor sector of fermion masses and mixing angles. Two decades of attempts to incorporate the standard model into a more fundamental and economical theory have resulted in just *one* highly significant quantitative success: the calculation of $\sin^2\theta_W$ in supersymmetric grand unified theories (GUT's) [1,2]. Although this is just one number, the quantitative agreement between theory and experiment is so precise that it constitutes an experimental hint in favor of low-energy supersymmetry. Furthermore, the prediction from supersymmetric GUT's has a much higher numerical significance than the prediction from superstrings [3].

The biggest obstacle to constructing a predictive theory is the flavor, or fermion mass, problem. Thirteen experimentally determined numbers are needed to phenomenologically parametrize this sector of the theory. But to make matters worse, with only 13 observables, the flavor sector is a highly underdetermined system, since, typically, many more parameters are needed to describe the Yukawa sector of some more fundamental theory. In order to make progress in this situation, one hopes that patterns in the masses and mixing angles can be explained by a few fundamental parameters. Tools that have been used to tackle this tough problem (and that minimize the number of fundamental parameters) include grand unification and family symmetries. Grand unification can, in principle, relate the lepton, up, and down mass matrices and hence reduce the number of input masses by a factor ~ 3. Family symmetry can enforce some zero entries in the Yukawa matrices, again limiting the number of fundamental parameters.

The consequences of the Georgi-Jarlskog ansatz [4] for Yukawa couplings in a supersymmetric theory were recently derived [5]. The ansatz included seven parameters in the Yukawa matrices plus one additional parameter entering the mass matrices, $\tan\beta$, the ratio of the vacuum expectation values (VEV's) of the two Higgs bosons present in any supersymmetric theory. With eight parameters, there are five predictions for fermion masses and mixing angles, and $\tan\beta$ is also predicted. These predictions are encouraging: in cases where they are already

*Present address: Department of Physics, Massachusetts Inst. of Technology, Cambridge, MA 02139.
†On leave, Theory Division, Los Alamos National Lab., Los Alamos, NM 87545.

tested they agree with the data at the 90% confidence level or better [5,6].

However, there are some shortcomings to this ansatz. (a) While down quark and charged lepton mass matrices are related, there are no relations between up and down quark masses, even within the context of an SO(10) [7] theory. (b) The ansatz parametrizes the fermion mass hierarchy (e.g., $m_\tau \gg m_\mu \gg m_e$), but it provides no understanding of the origin of this hierarchy. (c) Although the ansatz can be obtained from a set of family symmetries, it is nevertheless apparently *ad hoc*. Perhaps there are other equally successful *Ansätze* [8].

(d) There are seven parameters in the Yukawa matrices at $M_{\rm GUT}$. Can we find a theory with fewer parameters and thus more predictions?

Our approach builds on an earlier attempt to construct very predictive theories of fermion masses [9], in which four input parameters gave all quark and lepton masses and mixings. Although these earlier attempts were not completely successful, they did not incorporate *CP* violation and the top quark mass was too small, they did suggest a paradigm for theories of fermion masses which, as we show in this paper, are quite successful.

In this paper we make *a systematic operator analysis of the most predictive flavor sectors possible in supersymmetric grand unified SO(10) theories.*[1] The shortcomings mentioned above are addressed as follows.

(a) We exploit the full power of the SO(10) gauge symmetry obtaining relations between the up and down Yukawa matrices.

(b) The family hierarchy is related to the ratio of grand to Planck mass scales M_G/M_P.

(c) Instead of obtaining an example of a single predictive theory, we perform a systematic search for the most predictive flavor sectors within the SO(10) framework. We give general arguments as to the maximum number of predictions, and the search reveals all such theories.

(d) The minimal flavor structure involves just four SO(10) invariant operators. Since there is a single irremovable phase, the Yukawa matrices depend on only five parameters. Hence, these theories have three more predictions than the Georgi-Jarlskog *Ansatz*, and two more predictions than its SO(10) analog [4,5]. An analysis of the predictions reveals that some of these theories are already experimentally disfavored, while the others can be distinguished by future experiments.

Why should nature be so kind as to choose the GUT flavor sector to be maximally predictive? Such flavor sectors may be the only ones which can be significantly probed experimentally, but can they be motivated theoretically? It may be that the dominance of just four SO(10) invariant operators is a result of a set of family symmetries and the breaking pattern of these symmetries. This is an old idea [4,8–10]. Unfortunately, there is considerable freedom in choosing the family symmetries and the breaking pattern. Perhaps one day this will be understood in terms of a string compactification. There is certainly no guarantee that the set of symmetries resulting from a string theory will be very simple [11]. We give an explicit realization of how family symmetries can lead to our models, at least for the heavy two generations, in Appendix A. A more comprehensive development of such theories will be given elsewhere [12].

In Sec. II we discuss some virtues of the gauge group SO(10) and some features of the SO(10) interactions which generate quark and lepton interactions. In Sec. III we summarize the assumptions which lead to our class of predictive theories. We discuss the number of predictions in these theories and show that there are just two possible textures: the "22" and "23" textures. In Sec. IV we give the renormalization-group program which must be performed to derive the predictions for these theories, and discuss certain features common to both textures. In Sec. V an analytic analysis of the "22" texture is made, and nine models are discovered. The seven predictions of each of these models are derived using analytic approximations. Numerical predictions for the nine "22" models are given in Sec. VI, showing that some are already disfavored while others are successful. Section VII describes the result of a numerical search for theories with the "23" texture; although this texture necessarily has a certain degree of tuning, three models are found which agree well with data. Conclusions are given in Sec. VIII. Extensions of our ideas, and certain proofs, are left to appendixes.

II. FEATURES OF SO(10)

All our analysis is done within the context of a supersymmetric GUT, which breaks at the GUT scale to the minimal supersymmetric standard model (MSSM), thus preserving the good prediction for $\sin^2\theta_W$ [2]. The choice of GUT is constrained by our desire to relate up and down quark, as well as the charged lepton, mass matrices. The smallest grand unified symmetry that accomplishes this is SO(10), which has all the 16 chiral states of quarks and leptons (including the right-handed neutrino) that comprises one family fitting neatly into the 16-dimensional spinor representation. In this sense, SO(10) is quite unique since bigger groups containing one or more families in a single representation typically contain a plethora of unwanted and unobserved particles. The three 16-plets associated with the three known families will be denoted by $\mathbf{16}_1$, $\mathbf{16}_2$, and $\mathbf{16}_3$, the last being the heaviest.

Another virtue of SO(10) is that both Higgs bosons that occur in minimal supersymmetric theories can fit into *one* ten-dimensional representation of SO(10). This implies that the SO(10) invariant Yukawa interaction

$$O_{33} = A\,\mathbf{16}_3\ \mathbf{10}\ \mathbf{16}_3 \tag{2.1}$$

can give mass to the τ lepton, top and bottom quarks of the third family in terms of just *one* coupling A. This simple operator, first studied by Ananthanarayan, Lazarides, and Shafi [13], allows a prediction of the top quark mass from the bottom quark mass without any reference to the lighter generations. An interesting feature of this interaction is that the observed value of

[1] We do not include neutrino masses in our analysis, which would require the addition of further operators.

m_b/m_τ, forces the coupling A to be large, of order unity. In fact, the top quark mass in this scenario must be heavier than about 165 GeV [14]. The heaviness of the top quark is an immediate consequence of the large value for the third generation Yukawa coupling; now the question to ask is rather why the b and τ are so light. The large value for m_t/m_b can only be obtained by having a large ratio of electroweak VEV's $\tan\beta \equiv v_2/v_1 \approx m_t/m_b$ [15]. Such a large value of $\tan\beta$ requires a moderate fine-tuning in the MSSM which we do not discuss in this paper [16]. However, large $\tan\beta$ does have several important phenomenological consequences, one of which is the potentially very large weak-scale radiative correction to the down-type quark masses. At first sight these radiative corrections appear so large that they will destroy the top mass prediction. As discussed in Appendix D, this is typically not the case [14], and the effects of such corrections will be ignored in the results presented in this paper.

In addition to the Higgs decouplet **10** and three families $\mathbf{16}_1$, $\mathbf{16}_2$, and $\mathbf{16}_3$, more Higgs multiplets are certainly necessary to break SO(10) down to $SU(3)\times SU(2)\times U(1)$. These Higgs multiplets may enter the fermion mass matrices in operators with dimension (≥ 4). The smallest such representations are the **45** and the **16**. The **16** can reduce the rank, breaking SO(10) down to SU(5); it could also contribute to neutrino masses. The **45** can participate in several stages of SO(10) breaking depending on the direction in which it points. In concert, a **45**, **16**, and $\overline{\mathbf{16}}$ can break SO(10) to $SU(3)\times SU(2)\times U(1)$ [17].

Since the **45** is the adjoint representation of SO(10), its VEV can point in any direction in the space spanned by the 45 generators of SO(10) as long as it leaves the group $SU(3)\times SU(2)\times U(1)$ unbroken. This means that the **45** VEV lies in the two-dimensional subspace of $U(1)'$ generators of SO(10) that commute with $SU(3)\times SU(2)\times U(1)$. There are four special directions in this subspace.

(1) $\langle \mathbf{45} \rangle = v_{10} e^{i\phi_1} T_1 \equiv 45_1$. Here $v_{10}e^{i\phi_1}$ is the magnitude and phase of the VEV and $T_1 \equiv X$ is the SO(10) generator that commutes with the SU(5) Georgi-Glashow subgroup (the X quantum numbers of family members are shown in Table I). The reason why this direction is special is that it can break SO(10) down to $SU(5)\times U(1)_X$ at the scale v_{10}. The linearly independent direction is then given by

(2) $\langle \mathbf{45} \rangle = v_5 e^{i\phi_{24}} T_{24} \equiv 45_Y$. Here $T_{24} \equiv Y$ is the hypercharge generator and therefore it is not SU(5) invariant. The scale at which the three couplings, α_1, α_2, and α_3 unify is, by definition, the GUT scale, M_G. In this paper we assume $v_{10} \geq v_5$, resulting in a symmetry-breaking pattern

$$\mathrm{SO}(10) \xrightarrow{v_{10}} \mathrm{SU}(5) \xrightarrow{v_5} \mathrm{SU}(3)\times \mathrm{SU}(2)\times \mathrm{U}(1)_Y$$

where $v_5 \equiv M_{\mathrm{GUT}}$.

There is another special direction in this two-dimensional subspace:

(3) $\langle \mathbf{45} \rangle = v_5 e^{i\phi_{B-L}} T_{B-L} \equiv 45_{B-L}$. Here $B-L$ is simply the ordinary baryon minus lepton number. Although it is not linearly independent of the previous two directions, it may nevertheless play a significant dynamical role. It has been suggested before that this VEV might naturally induce the necessary doublet-triplet splitting in the Higgs sector [18]. Once again, since this VEV breaks SU(5), we shall assume that the magnitude of its VEV is given by $v_5 = M_G$.

Finally, the linearly independent direction is as follows:

(4) $\langle \mathbf{45} \rangle = v_5 e^{i\phi_{3R}} T_{3R} \equiv 45_{T_{3R}}$. T_{3R} is the third component of the right-handed isospin group. It also breaks SU(5) and so we have again assumed that it has a VEV of magnitude v_5.

In any complete SO(10) model, additional Higgs in 54- or 210-dimensional representations may be necessary to force the desired breaking pattern. We shall not consider these states in our analysis. As discussed, we have identified $v_5 = M_G$. As for the scale v_{10}, we will assume that it can take values anywhere between the Planck mass M_P and M_G.

The effective theory near the scale M_G will then consist of renormalizable terms plus higher dimension operators suppressed by powers of either v_5/M_P, v_{10}/M_P, or v_5/v_{10}.[2] In particular, there are higher dimension operators of the form

$$O_{ij} \equiv \mathbf{16}_i \frac{\mathbf{45}_1}{M_1} \cdots \frac{\mathbf{45}_k}{M_k} \mathbf{10} \frac{\mathbf{45}_{k+1}}{M_{k+1}} \cdots \frac{\mathbf{45}_l}{M_l} \mathbf{16}_j \,, \qquad (2.2)$$

where some of the M_n in the denominator can be $\sim M_P$ and others $\sim v_{10}$, and $i,j = 1,2,3$. In writing these operators we understand the SO(10) group invariant to be formed as follows: use the SO(10) γ matrices to write the **45** and **10** as 16×16 matrices and then compute the invariant by a succession of matrix multiplications. The operators so formed are those which result from integrating out heavy **16** and $\overline{\mathbf{16}}$, as shown by an example in Appendix A. Other group contractions are possible, for example, by integrating out a heavy **144**, but we do not include these operators in this paper. We seek the predictive flavor sectors which could result from only the simplest GUT's.

When the **45**'s get VEV's (in any of the four preferred directions $\mathbf{45}_1$, $\mathbf{45}_Y$, $\mathbf{45}_{B-L}$, $\mathbf{45}_{T_{3R}}$) these operators contribute to the ijth element of the mass matrices of charged leptons and up and down quarks. These contri-

TABLE I. Quantum numbers.

	X	Y	$B-L$	T_{3R}
q	1	1	1	0
u^c	1	−4	−1	1
d^c	−3	2	−1	−1
l	−3	−3	−3	0
e^c	1	6	3	−1
ν^c	5	0	3	1

[2]These higher dimension operators may, in principle, be obtained by integrating out heavy states at the scales v_{10} or M_P. See Appendix A for more details of such an interpretation.

butions are very simply related to each other: every time a **45** VEV couples to a quark or lepton it just counts its X, Y, $(B-L)$, or T_{3R} charge (shown in Table I) depending on whether the VEV points in the $\mathbf{45}_1$, $\mathbf{45}_Y$, $\mathbf{45}_{(B-L)}$, or $\mathbf{45}_{T_{3R}}$ direction. Thus, armed with this table, and for any choice of the VEV's, we can easily compute the contribution of the operator (2.2) to lepton or up and down quark mass matrices.

In these models, the fermion mass hierarchy originates from a hierarchy of mass scales: $v_5 = M_G \leq v_{10} \leq M_P$.

III. A CLASS OF PREDICTIVE THEORIES

A. The assumptions

Our objective is to construct the most economical and predictive class of theories of quark and lepton masses. This clearly involves making a set of assumptions, which we now summarize.

(1) We require a supersymmetric GUT to preserve the successful prediction for $\sin^2\theta_W$, as discussed earlier, and SO(10) is taken as the gauge group, since it is the smallest group relating leptons and up and down quarks with no superfluous particles.

(2) Beneath the GUT scale the effective theory is taken to be the MSSM.

(3) The two Higgs doublets that occur in the MSSM both belong to a unique **10** of SO(10). This leads to an economy of parameters: for example, the single Yukawa coupling A of Eq. (2.1) is responsible for the masses of three fermions of the third generation: t, b, and τ.

(4) All dimensionless couplings of the GUT should be of order unity. This implies that only the third family, $\mathbf{16}_3$, gets a mass via a renormalizable operator having dimension $d \leq 4$. Given the previous assumption, this operator is necessarily that of Eq. (2.1).

(5) All lighter families get their mass via the higher dimension operators O_{ij} of Eq. (2.2). Recall that the M_n's in the denominators emerge from physics beyond M_G (for more details on this point, see Appendix A). Some of the M_n's are $\sim M_P$ and others are proportional to $\langle \mathbf{45}_1 \rangle$ and therefore $\sim v_{10}$. The ratio of scales will provide a partial understanding of the fermion mass hierarchy. These ratios are bounded, since the lower scale $M_G \sim 10^{16}$ GeV and $M_P \sim 10^{18}$ GeV.

(6) Each of the $\langle \mathbf{45}_n \rangle$'s [occurring in the numerator of the operators O_{ij} of Eq. (2.2)] can only point in one of the four directions $\mathbf{45}_1$, $\mathbf{45}_Y$, $\mathbf{45}_{(B-L)}$, and $\mathbf{45}_{T_{3R}}$ introduced in Sec. II. This hypothesis is often satisfied in specific SO(10) models. The reason is that, as mentioned in Sec. II, these VEV's accomplish a very specific step on the breaking chain of SO(10) down to $SU(3)\times SU(2)\times U(1)$. In some cases this hypothesis is a corollary of the more general extended survival hypothesis [19].

(7) The charged lepton masses and the quark masses and mixings are assumed to be described, to a certain level of accuracy, by the smallest number of SO(10) invariant operators possible. Such a picture may emerge from a pattern of spontaneously broken family symmetries.

(8) The parameters of the MSSM are taken such that the one-loop weak-scale radiative corrections to the masses of the down-type quarks and charged leptons can be neglected. We have argued in Appendix D why this is expected to be true when $\tan\beta$ is large.

B. The operator search

This is a long list of assumptions: without a fundamental theory of fermion masses some such list is always necessary. We believe that each assumption is reasonable and are encouraged by the success of the scheme. Some of the assumptions, for example, (3) and (7), are strong, but we should stress that not all assumptions are needed for each prediction. In fact, for any one of our predictions a weaker set of assumptions can be formulated. However, we believe that we have given the minimal set of assumptions for all seven flavor predictions to result from the same theory.

Using the above assumptions we can now begin to construct theories of fermion masses. We first show that the minimal texture of this type includes just four effective operators.

In the absence of the nonrenormalizable operators O_{ij} of Eq. (2.2) it is clear that only the third generation τ, t, and b fermions will acquire mass via the operator of Eq. (2.1). The physical quantities of interest in this sector are four: m_τ, m_t, m_b, and $\tan\beta$. These are given in terms of the Yukawa coupling A and $\tan\beta$. Following Ananthanarayan, Lazarides, and Shafi (ALS) [13], we use the experimental values for m_b/m_τ and m_τ to fix A at M_G. We then predict m_t and $\tan\beta$. The results are shown in Fig. 1 as a function of m_b for various values of $\alpha_s(M_Z)$. It is important to note that for α_s in the range $0.11 \leq \alpha_s \leq 0.13$, the top mass comes out heavier than ~ 160 GeV. If the top is lighter than 160 GeV, then at least one of assumptions (3) and (8) must be incorrect.

Now we come to the two lighter families. It is clear that there must be a minimum of two operators of the form of Eq. (2.2) in order for the mass matrices to have a nonzero determinant, which is necessary to ensure that the electron is not massless. If there were only two such operators, they would necessarily be O_{23} and O_{12} which give rise to V_{cb} and V_{us}, respectively. Note that we cannot replace O_{12} and O_{13}, since the resulting V_{us} would be too small. These operators O_{23} and O_{12} together with the Yukawa coupling of Eq. (2.1) are *not* enough: in Appendix B we show that if O_{23} is of dimension 5 or 6, agreement with the observed masses and mixings of the heavy two families cannot be obtained. It is shown that an additional operator must contribute either to the 22 entry or to the 23 entry. A corollary of this theorem is that our theories have Kobayashi-Maskawa-type CP violation. This is because the phases of the Yukawa coupling, A, and the three effective Yukawa couplings, resulting from the higher dimension operators cannot all be removed by redefining the phases of $\mathbf{16}_1$, $\mathbf{16}_2$, and $\mathbf{16}_3$. We thus conclude that the minimal texture includes four effective operators, which result in six arbitrary parameters in the fermion mass matrices (four magnitudes and one phase in the Yukawa matrices and $\tan\beta$). We will thus have seven flavor predictions. We can have the two

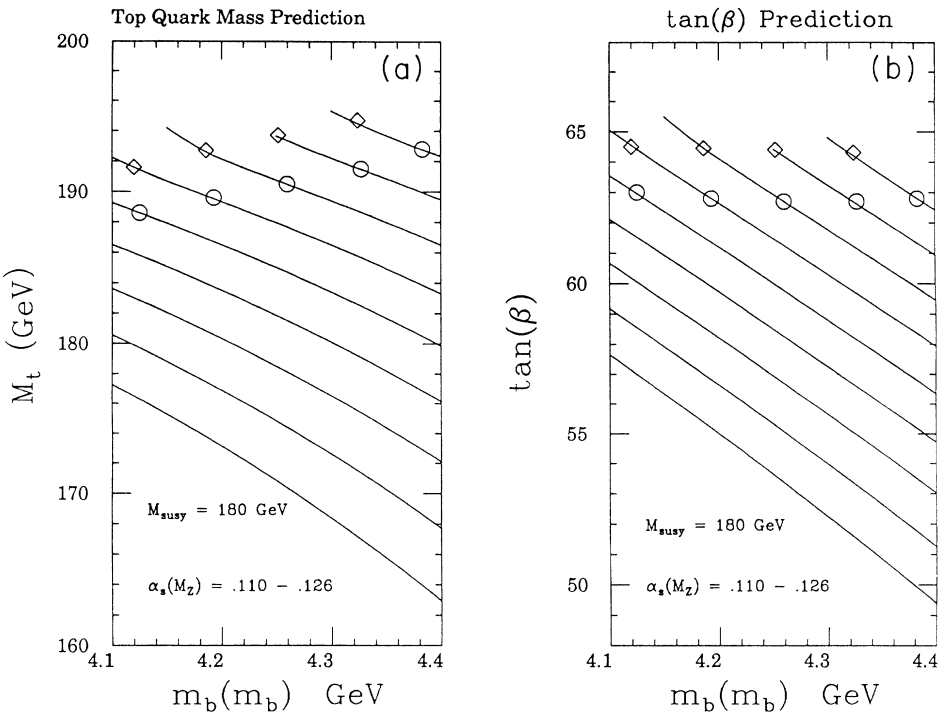

FIG. 1. (a) The physical top quark mass prediction is plotted as a function of the $\overline{\text{MS}}$ value of the bottom quark mass for $\alpha_s(M_Z)=0.110$–0.126. M_t is an increasing function of α_s. The circles (diamonds) represent points where the GUT-scale Yukawa coupling is equal to 2 (3). (b) The ratio of vacuum expectation values, $\tan\beta$, is plotted as a function of the $\overline{\text{MS}}$ value of the bottom quark mass for $\alpha_s(M_Z)=0.110$–0.126. $\tan\beta$ is an increasing function of α_s. The circles (diamonds) represent points where the GUT-scale Yukawa coupling is equal to 2 (3).

possible textures defined by

$$O_{33}+O_{23}+O_{22}+O_{12} \tag{3.1}$$

or

$$O_{33}+O^a_{23}+O^b_{23}+O_{12}\ . \tag{3.2}$$

IV. RENORMALIZATION GROUP, O_{33} AND O_{12}

In this section we consider the renormalization-group (RG) evolution of the Yukawa eigenvalues and mixing angles from the GUT scale to low energies. We make use of well-known simple one-loop formulas to scale from grand to weak scales, M_G to M_S [20,25], which include the effects of large t, b, and τ Yukawa couplings. These results will be used in the next section. In the numerical analyses of Secs. VI and VII a two-loop renormalization-group (RG) analysis is performed. In this section we also discuss O_{33} and O_{12} which are unique and therefore common to both textures.

The third generation Yukawas at the weak scale are

$$\lambda_t=\lambda_{t_G}\prod_a \zeta_a^u e^{-6I_t-I_b}\ , \tag{4.1a}$$

$$\lambda_b=\lambda_{b_G}\prod_a \zeta_a^d e^{-I_t-6I_b-I_\tau}\ , \tag{4.1b}$$

$$\lambda_\tau=\lambda_{\tau_G}\prod_a \zeta_a^e e^{-3I_b-4I_\tau}\ , \tag{4.1c}$$

where the subscript G refers to the GUT scale. The integrals I_i are given by

$$I_i=\int_{\ln M_S}^{\ln M_G}\left[\frac{\lambda_i(t)}{4\pi}\right]^2 dt \tag{4.2}$$

and are shown in Fig. 2 for $i=t,b,\tau$. The gauge coupling renormalizations are given by the ζ_a^i factors, where i refers to u, d, e flavor and $a=1,2,3$ to the gauge group U(1), SU(2), or SU(3):

$$\zeta_a^i=\left[\frac{\alpha_G}{\alpha_a}\right]^{c_a^i/2b_a}\ , \tag{4.3}$$

where $c_a^u=(\frac{13}{15},3,\frac{16}{3})$, $c_a^d=(\frac{7}{15},3,\frac{16}{3})$, and $c_a^e=(\frac{27}{15},3,0)$. The one-loop gauge β-function coefficients are $b_a=(\frac{33}{5},1,-3)$. We remind the reader that M_S is the effective scale of supersymmetry breaking, and above this scale our theory has the particle content of the minimal supersymmetric standard model up to mass scale M_G. In

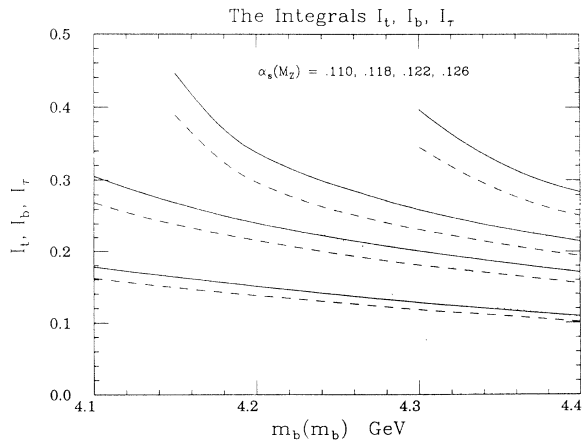

FIG. 2. The integrals I_t, I_b, and I_τ. I_t (solid curve), I_b (dashed curve), and I_τ (dotted curve), are plotted as of function of the $\overline{\text{MS}}$ value of the bottom quark mass.

this section we ignore GUT and supersymmetric threshold correction effects, which we expect to affect our predictions at the level of 7%.

In analytic results given later in the paper the running of the gauge couplings is treated as follows. At $\mu=M_Z$ we input $\alpha_1^{-1}=58.8$ and $\alpha_2^{-1}=29.8$ but keep $\alpha_3(M_Z)$ a free parameter. Except for a special value of $\alpha_3(M_Z)$ (0.108) the three gauge couplings do not exactly meet at the GUT scale. This we assume to be due to GUT threshold corrections. This allows us to show how our predictions vary with $\alpha_3(M_Z)$. We assume that the GUT mass relations are valid at a scale $M_G=2\times10^{16}$ GeV. This could also be affected by GUT threshold corrections, but is unlikely to change our predictions by more than a few percent.

The RG scaling of masses of lighter generations are best shown as mass ratios, as this removes the ζ_a^i factors

$$\frac{\lambda_{u,c}}{\lambda_t}=\left[\frac{\lambda_{u,c}}{\lambda_t}\right]_G e^{3I_t+I_b}, \tag{4.4a}$$

$$\frac{\lambda_{d,s}}{\lambda_b}=\left[\frac{\lambda_{d,s}}{\lambda_b}\right]_G e^{I_t+3I_b}, \tag{4.4b}$$

$$\frac{\lambda_{e,\mu}}{\lambda_\tau}=\left[\frac{\lambda_{e,\mu}}{\lambda_\tau}\right]_G e^{3I_\tau}. \tag{4.4c}$$

We remind the reader that in these formulas the Yukawa couplings λ_i are the eigenvalues of the Yukawa matrices at scale $\mu=M_S$.

The scaling of the Kobayashi-Maskawa (KM) matrix elements is extremely simple:

$$V_{cb}=V_{cb_G}e^{I_t+I_b} \tag{4.5}$$

and identical behavior for V_{ub}, V_{ts}, and V_{td}. The *CP*-violating quantity J scales as V_{cb}^2: i.e.,

$$J=J_G e^{2I_t+2I_b}. \tag{4.6}$$

To the level which we work, the following quantities are RG invariant: V_{us}, V_{cd}, V_{ud}, V_{cs}, V_{tb}, λ_u/λ_c, λ_d/λ_s, and λ_e/λ_μ.

Finally, we must compare our predictions at M_S with parameters extracted from experiment. Since M_S is close to the weak scale, we compare the elements of the KM matrix at M_S directly with those determined experimentally. Similarly, we take the running top mass to be

$$m_t\simeq\lambda_t(M_S)\frac{v}{\sqrt{2}}\sin\beta \tag{4.7}$$

and the "physical" top mass as

$$M_t\simeq m_t\left[1+\frac{4}{3}\frac{\alpha_s(m_t)}{\pi}\right]. \tag{4.8}$$

Hence we are choosing M_S to be in the neighborhood of the top mass; for definiteness we take 180 GeV.

The other fermion masses require that we RG scale the Yukawa parameters below M_S. We define RG scaling parameters η_i by

$$m_i(m_i)\equiv\eta_i m_i(M_S) \tag{4.9a}$$

for all quarks and leptons except u, d, and s quarks which have η_i defined by

$$m_i(1\text{ GeV})\equiv\eta_i m_i(M_S)\quad i=u,d,s. \tag{4.9b}$$

Plots of η_i are shown in Fig. 3 for $i=u,d,s,c,b$ where the QCD contribution has been calculated to three loops. We also include one-loop QED contributions to the η_i.

We now turn to a discussion of the degree to which each of the four SO(10) operators which contribute to fermion masses have a unique SO(10) structure. We first discuss the 33 operator. There are two possibilities for a renormalizable 33 operator in SO(10): $\mathbf{16}_3\ \mathbf{10}\ \mathbf{16}_3$ and $\mathbf{16}_3\ \overline{\mathbf{126}}\ \mathbf{16}_3$. The latter case implies $\lambda_{\tau_G}=3\lambda_{b_G}$, which can only be turned into a successful m_b/m_τ relation if α_s is large and if m_b is less than about 4.0 GeV [14].[3] While this case is not excluded, we have chosen to use the operator $\mathbf{16}_3\ \mathbf{10}\ \mathbf{16}_3$ in this paper, since this is known to work very well [13]. The grand unified boundary condition on the three Yukawa couplings of the heaviest generation,[4] $\lambda_{t_G}=\lambda_{b_G}=\lambda_{\tau_G}$, is reminiscent of that for the three gauge couplings $g_{1_G}=g_{2_G}=g_{3_G}$. The two free parameters, A and $\tan\beta$, are determined by m_b and m_τ via

$$\frac{m_b}{m_\tau}=\frac{\eta_b}{\eta_\tau}\prod_a\left[\frac{\zeta_a^d}{\zeta_a^e}\right]e^{-I_t-3I_b+3I_\tau} \tag{4.10}$$

for A and

$$m_\tau=\frac{v}{\sqrt{2}}\cos\beta A\eta_\tau\prod_a\zeta_a^e e^{-3I_b-4I_\tau} \tag{4.11}$$

for $\tan\beta$. The two predictions for M_t and $\tan\beta$, cannot be given in simple analytic equations, and are shown in Figs. 1(a) and 1(b) as a function of the input m_b for various α_s.

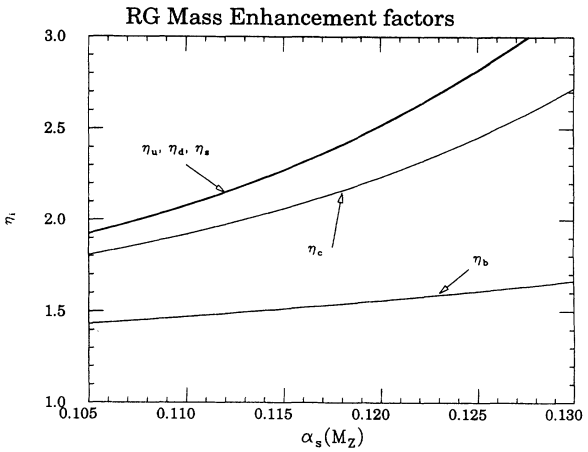

FIG. 3. The renormalization-group mass enhancement factors η_i are plotted as a function of $\alpha_s(M_Z)$. $\eta_i=m_i(m_i)/m_i(m_S)$ for $i=c$, b, and $\eta_i=m_i(1\text{ GeV})/m_i(m_S)$ for $i=u,d,s$.

[3]This could, perhaps, be overcome by large weak-scale radiative corrections to the b quark mass.

[4]There are perturbative corrections to this formula.

In our "analytic" analysis for the lighter generation we will read I_i, m_t, and $\tan\beta$ from Figs. 1, 2, and 3 and will never actually use (4.10) or (4.11). Note that the values of M_t which we predict are larger than those given by Ananthanarayan, Lazarides, and Shafi, partly because they used values of α_s which would be considered low today.

In Appendix C we prove that, once the 33 operator has been chosen to be $\mathbf{16}_3\ \mathbf{10}\ \mathbf{16}_3$, the choice for the 12 entry is unique. The experimental inputs needed to obtain this result are quite mild:

$$60\ \text{MeV} < m_s < 360\ \text{MeV}\ ,$$
$$0.2 < m_u/m_d < 1.5\ ,$$

and the experimental value for the Cabibbo angle. The resulting operator is

$$O_{12} = \mathbf{16}_1 \left[\frac{\mathbf{45}_1}{M}\right]^3 \mathbf{10} \left[\frac{\mathbf{45}_1}{M}\right]^3 \mathbf{16}_2\ , \tag{4.12}$$

which yields symmetric entries, i.e., the 12 and 21 entries are equal in each mass matrix.

In our scheme the large value of m_t/m_b results from a hierarchy in the doublet VEV's, $\tan\beta \gg 1$. One might then expect that this hierarchy of VEV's would lead to large values for both m_c/m_s and m_u/m_d. However, m_u/m_d is of order unity and is an order of magnitude or more smaller than m_c/m_s and m_t/m_b. How does our theory solve this mystery of why $m_u < m_d$ while $m_c \gg m_s$ and $m_t \gg m_b$? The answer is yet again a Clebsch factor of 3. Every **45**, appearing in O_{12} of Eq. (4.12) contributes a factor of 3 to $z_d z_d'/z_u z_u'$. Hence, from the determinant of the up and down Yukawa matrices we derive

$$\frac{m_u}{m_d} = \left[\frac{m_t}{m_b}\right]^2 \left[\frac{m_s}{m_c}\right] \left|\frac{z_u z_u'}{z_d z_d'}\right| \frac{\eta_b^2 \eta_u \eta_c}{\eta_d \eta_s} e^{4(I_t - I_b)}\ . \tag{4.13}$$

Thus the naive expectation of

$$m_u/m_d \simeq (m_t/m_b)^2 (m_s/m_c) \simeq 200$$

is actually enhanced by RG effects by a factor of about 2–3 to become of order 400–600. It is the Clebsch of

$$\left|\frac{z_u z_u'}{z_d z_d'}\right| = \frac{1}{3^6} \simeq 10^{-3}\ ,$$

which reduces m_u/m_d to around 0.6–0.8. Because the RG enhancement is smallest for small values of $\alpha_s(M_Z)$ the prediction for m_u/m_d favors smaller values of the strong-coupling constant.

The operator (4.12) involves six suppression factors of $\langle \mathbf{45}_1 \rangle / M$. This implies that the scale at which SO(10) is broken to SU(5)×U(1) by $\langle \mathbf{45}_1 \rangle$ is not much less than the fundamental mass scale of the theory, M.

We have shown that O_{33} and O_{12} are unique, and thus identical in "22" and "23" models. To go further we must treat the "22" and "23" textures separately.

V. THE "22" TEXTURE

In this section we present an analytic treatment of models based on the "22 texture" shown in Eq. (3.1), and so called because there is an operator which contributes to the 22 entry of the mass matrices. We first give the general form of Yukawa matrices of these theories and show how they may be approximately diagonalized at the GUT scale. In the last section we showed that O_{33} and O_{12} are unique. In Appendix D, a numerical search is described which proves that the Clebsch structure of the 22 entries is also unique. This allows us to prove that there are just nine possible operators for the 23 entry, and hence nine possible models. We show how m_e, m_μ, m_τ, m_c, m_b, and the Cabibbo angle can be used to accurately determine the six free parameters which describe the flavor sector of these theories, and give the resulting eight predictions of the flavor sector. We find that m_s/m_d disfavors some of the models. In addition, we give the predictions of these models for the kaon CP impurity parameter ϵ, for $B^0\overline{B^0}$ mixing, and for the CP-violating asymmetries in neutral B meson decay.

The GUT scale Yukawa matrices which follow from the theories defined by the four operators of Eq. (3.1) can be written in the form

$$\lambda_i = \begin{pmatrix} 0 & z_i' C & 0 \\ z_i C & y_i E e^{i\tilde{\phi}} & x_i' B \\ 0 & x_i B & A \end{pmatrix}\ , \tag{5.1}$$

where $i = u, d, e$. In this paper we define the coupling matrices with the doublet fields to the right of the matrices, so x_i are relevant for V_{cb}.

Notice that A, B, E, and C are all dimensionless: they are the original operator coefficients multiplied by the relevant factor of **45** vacuum expectation values. Thus $A \gg B$ and $E \gg C$. Phase redefinitions on the matter multiplets have been arranged so that the single physical phase $\tilde{\phi}$ appears in the 22 entry. The Clebsch factors from the **45** VEV's are parametrized as x_i, x_i', y_i, z_i, and z_i' and for a given model can be obtained from Table I.

Approximate diagonal forms for these matrices at the GUT scale can be obtained by the following sequence of transformations: (i) In the heavy 2×2 sector rotate the left-handed fermions by angles $\alpha_i = x_i B/A$, and the right-handed ones by $\alpha_i' = x_i' B/A$; (ii) write the resulting 22 entry as $y_i E_i e^{i\phi_i}$ and rotate the left- and right-handed lightest generation fermions by a phase factor $e^{i\phi_i}$; (iii) diagonalize the light 2×2 sector by rotations $\beta_i = z_i C/y_i E_i$ and $\beta_i' = z_i' C/y_i E_i$ on the left- and right-handed fermions, respectively.

Let $\bar{\theta}_3 = -\alpha_u$, $\bar{\theta}_4 = -\alpha_d$, $\theta_2 = -\beta_u$, and $\theta_1 = \beta_d$; then the transformations in the left-handed up and down sectors are

$$V_u = \begin{pmatrix} c_2 & s_2 & 0 \\ -s_2 & c_2 & 0 \\ 0 & 0 & 1 \end{pmatrix} \begin{pmatrix} e^{i\phi_u} & 0 & 0 \\ 0 & 1 & 0 \\ 0 & 0 & 1 \end{pmatrix} \begin{pmatrix} 1 & 0 & 0 \\ 0 & \overline{c_3} & \overline{s_3} \\ 0 & -\overline{s_3} & \overline{c_3} \end{pmatrix} \tag{5.2a}$$

and

$$V_d=\begin{bmatrix} c_1 & -s_1 & 0 \\ s_1 & c_1 & 0 \\ 0 & 0 & 1 \end{bmatrix}\begin{bmatrix} e^{i\phi_d} & 0 & 0 \\ 0 & 1 & 0 \\ 0 & 0 & 1 \end{bmatrix}\begin{bmatrix} 1 & 0 & 0 \\ 0 & \overline{c_4} & \overline{s_4} \\ 0 & -\overline{s_4} & \overline{c_4} \end{bmatrix} . \tag{5.2b}$$

Setting $\theta_3=\overline{\theta_3}-\overline{\theta_4}$ and $\phi=\phi_u-\phi_d$, the KM matrix takes the form

$$V=V_u V_d^{\dagger}=\begin{bmatrix} c_1c_2-s_1s_2e^{-i\phi} & s_1+c_1s_2e^{-i\phi} & s_2s_3 \\ -c_1s_2-s_1e^{-i\phi} & c_1c_2c_3e^{-i\phi}-s_1s_2 & c_2s_3 \\ s_1s_3 & -c_1s_3 & c_3e^{i\phi} \end{bmatrix} , \tag{5.3}$$

which is identical in form to the KM matrix obtained in a previous framework [5]. The angles θ_1 and θ_2 are related to quark Yukawa couplings and the Clebsch factors z_i and z_i' by

$$s_1=\left[\left|\frac{z_d}{z_d'}\right|\right]^{1/2}\left[\frac{\lambda_d}{\lambda_s}\right]^{1/2} ,$$
$$s_2=\left[\left|\frac{z_u}{z_u'}\right|\right]^{1/2}\left[\frac{\lambda_u}{\lambda_c}\right]^{1/2} .$$

Using results from the last section it is straightforward to see that θ_1, θ_2, and ϕ are RG invariants, while s_3 scales as V_{cb}.

We now turn to a discussion of the 22 and 23 operators, which generate V_{cb_G}, λ_{c_G}, λ_{s_G}, and λ_{μ_G}. The low-energy experimental values of $V_{cb}=0.044\pm0.006$, $m_c=1.22\pm0.05$ GeV, $m_s=175\pm55$ MeV, and $m_\mu=106$ MeV can be run up to the GUT scale with the RG equations yielding

$$V_{cb_G}=0.040-0.024 , \tag{5.4a}$$
$$\left[\frac{\lambda_c}{\lambda_t}\right]_G=0.0030-0.0012 , \tag{5.4b}$$
$$\left[\frac{\lambda_s}{\lambda_b}\right]_G=0.025-0.009 , \tag{5.4c}$$
$$\left[\frac{\lambda_\mu}{\lambda_\tau}\right]_G=0.048-0.035 , \tag{5.4d}$$

where the quoted ranges correspond to $\alpha_s(M_Z)=0.11-0.13$, respectively. In the cases of (5.4b)–(5.4d) we have also used our prediction for m_t and inputs $m_b=4.15\pm0.1$ GeV and $m_\tau=1.78$ GeV. A crucial feature concerning the magnitude of these four quantities is

$$V_{cb_G}^2\simeq\left|\frac{\lambda_c}{\lambda_t}\right|_G\ll\left|\frac{\lambda_\mu}{\lambda_\tau}\right|_G\simeq 3\left|\frac{\lambda_s}{\lambda_b}\right|_G . \tag{5.4e}$$

The theory can naturally account for this division into two small parameters and two large ones if the 23 operator generates the small parameters and the 22 operator the large ones. This requires a 22 operator which gives $|y_u|:|y_d|:|y_e|=<\frac{1}{3}:1:3$. A study of all operators at dimensions 5 and 6 shows there to be a unique y_i which satisfies this:

$$y_u:y_d:y_e=0:1:3 . \tag{5.5}$$

This is the form familiar from the Georgi-Jarlskog texture. There are six operators which give such Clebsch ratios

$$\mathbf{16}_2\mathbf{45}_1\mathbf{10}\frac{\mathbf{45}_{B-L}}{\mathbf{45}_1}\mathbf{16}_2 , \tag{5.6a}$$
$$\mathbf{16}_2\frac{\mathbf{1}}{\mathbf{45}_1}\mathbf{10}\,\mathbf{45}_{B-L}\mathbf{16}_2 , \tag{5.6b}$$
$$\mathbf{16}_2\mathbf{45}_1\mathbf{10}\,\mathbf{45}_{B-L}\mathbf{16}_2 , \tag{5.6c}$$
$$\mathbf{16}_2\mathbf{10}\frac{\mathbf{45}_{B-L}}{\mathbf{45}_1}\mathbf{16}_2 , \tag{5.6d}$$
$$\mathbf{16}_2\mathbf{10}\,\mathbf{45}_1\mathbf{45}_{B-L}\mathbf{16}_2 , \tag{5.6e}$$
$$\mathbf{16}_2\mathbf{10}\frac{\mathbf{45}_{B-L}}{\mathbf{45}_1^2}\mathbf{16}_2 . \tag{5.6f}$$

Since they lead to the same $y_u:y_d:y_e$, the operators lead to identical predictions. All six operators require a $\mathbf{45}_{B-L}$ in addition to the $\mathbf{45}_1$, which is needed both here and for O_{12}.

The 23 operator generates not only

$$V_{cb_G}=(x_d-x_u)\frac{B}{A} , \tag{5.7}$$

but is also entirely responsible for generating λ_{c_G}:

$$\left[\frac{\lambda_c}{\lambda_t}\right]_G=|x_ux_u'|\left[\frac{B}{A}\right]^2 . \tag{5.8}$$

Since B/A is determined by the charm quark mass, the Clebsch combinations x_ux_u' and x_u-x_d cannot both be independently probed. Eliminating B/A gives

$$V_{cb_G}=\chi\left[\left|\frac{\lambda_c}{\lambda_t}\right|_G\right]^{1/2} , \tag{5.9}$$

where the Clebsch combination which can be measured is given by

$$\chi\equiv\frac{|x_u-x_d|}{\sqrt{|x_ux_u'|}} \tag{5.10}$$

and the sign of B/A was chosen to make V_{cb} positive. Experimental values for V_{cb} and m_c, together with the predicted value of $m_t(\alpha_s)$ imply that allowed values of χ must fall in the range

$$0.55<\chi<0.92 , \tag{5.11}$$

where the larger values of χ tend to result from large V_{cb} and large α_s.

A search of all operators of dimensions 5 and 6 shows that only three values of χ occur in this range: $\chi=\frac{2}{3}$, $\frac{5}{6}$,

and $\frac{8}{9}$, resulting from the following operators:

$\chi=\frac{2}{3}$:

$$(1)\ \mathbf{16}_2\mathbf{45}_{24}\mathbf{10}\frac{\mathbf{1}}{\mathbf{45}_1}\mathbf{16}_3\ ,$$

$$(2)\ \mathbf{16}_2\mathbf{45}_{24}\mathbf{10}\frac{\mathbf{45}_{B-L}}{\mathbf{45}_1}\mathbf{16}_3\ , \tag{5.12a}$$

$$(3)\ \mathbf{16}_2\frac{\mathbf{45}_{24}}{\mathbf{45}_1}\mathbf{10}\frac{\mathbf{1}}{\mathbf{45}_1}\mathbf{16}_3\ ,$$

$$(4)\ \mathbf{16}_2\frac{\mathbf{45}_{24}}{\mathbf{45}_1}\mathbf{10}\frac{\mathbf{45}_{B-L}}{\mathbf{45}_1}\mathbf{16}_3\ ;$$

$\chi=\frac{5}{6}$:

$$(5)\ \mathbf{16}_2\mathbf{45}_{24}\mathbf{10}\frac{\mathbf{45}_{24}}{\mathbf{45}_1}\mathbf{16}_3\ , \tag{5.12b}$$

$$(6)\ \mathbf{16}_2\frac{\mathbf{45}_{24}}{\mathbf{45}_1}\mathbf{10}\frac{\mathbf{45}_{24}}{\mathbf{45}_1}\mathbf{16}_3\ ;$$

$\chi=\frac{8}{9}$:

$$(7)\ \mathbf{16}_2\mathbf{10}\frac{\mathbf{1}}{\mathbf{45}_1^2}\mathbf{16}_3\ ,$$

$$(8)\ \mathbf{16}_2\mathbf{10}\frac{\mathbf{45}_{B-L}}{\mathbf{45}_1^2}\mathbf{16}_3\ , \tag{5.12c}$$

$$(9)\ \mathbf{16}_2\mathbf{10}\frac{\mathbf{45}_{B-L}^2}{\mathbf{45}_1^2}\mathbf{16}_3\ .$$

In Eqs. (5.12) we label the operators (1)–(9) and will use these numbers also to denote the corresponding models. If slightly larger values of V_{cb} and α_s are accepted, the case $\chi=1$ is also allowed.[5] This case has been studied previously [6] and arises when $\lambda_{t_G}=\lambda_{b_G}$ is imposed on the Georgi-Jarlskog texture, which has $x_d=0$ and $x_u'=x_u$ and, therefore, $\chi=1$. It is interesting to note that this can be quite simply obtained by the operator

$$\mathbf{16}_2\mathbf{10}\ \mathbf{45}_1\mathbf{45}_Y\mathbf{16}_3\ . \tag{5.13}$$

At first sight, the Georgi-Jarlskog texture seems to be in conflict with the idea of up-down SO(10) mass relations: $U_{22}=0$ but $D_{22}\neq 0$, and $U_{23}\neq 0$ but $D_{23}=0$. We find that this is not the case. The Georgi-Jarlskog predictions result with the 23 operator of Eq. (5.13) and any of the 22 operators of (5.6). The condition $\lambda_{t_G}=\lambda_{b_G}$, which was not part of the original Georgi-Jarlskog scheme, implies that $\chi=1$ results only if α_s and V_{cb} are uncomfortably large, so we do not consider it further.

We have written down the most general set of 22 and 23 operators which follow from the assumption that λ_{μ_G} and λ_{s_G} are dominated by the 22 operator, while λ_{c_G} and V_{cb_G} have contributions only from the 23 operator. While we have argued that this is a natural division, it is not obvious that it is a necessary one. In Sec. VI we mention a numerical search for all possible models with the texture of (5.1) with the z_i and z_i' Clebsch factors coming from operator (4.12), which we have already proved is unique. The result of this numerical search is just the models described by the 22 operators of Eq. (5.6) and the 23 operators of Eq. (5.12). These well-motivated models are the unique ones of this texture.

Thus, without any loss of generality, we are now able to write the GUT-scale Yukawa matrices which result from this texture as

$$\mathbf{U}=\begin{pmatrix} 0 & -\frac{1}{27}C & 0 \\ -\frac{1}{27}C & 0 & x_u'B \\ 0 & x_uB & A \end{pmatrix},$$

$$\mathbf{D}=\begin{pmatrix} 0 & C & 0 \\ C & Ee^{i\tilde{\phi}} & x_d'B \\ 0 & x_dB & A \end{pmatrix}, \tag{5.14}$$

$$\mathbf{E}=\begin{pmatrix} 0 & C & 0 \\ C & 3Ee^{i\tilde{\phi}} & x_e'B \\ 0 & x_eB & A \end{pmatrix}.$$

The unique z_i,z_i',y_i,y_i' Clebsch factors have been shown explicitly, while the x_i,x_i' parameters allow for the possible Clebsch factors which follow from the 23 operators of Eq. (5.12).

The fermion masses and mixing angles depend on six free parameters: A, B, C, E, $\tilde{\phi}$, and $\tan\beta$. We will now give the six equations that fix these parameters in terms of m_e, m_μ, m_τ, m_c, m_b, and $\sin\theta_C$. A and $\tan\beta$ are given in terms of m_b and m_τ in Eqs. (4.10) and (4.11). B/A is determined from m_c via the equation

$$\frac{m_c}{m_t}=\eta_c|x_ux_u'|\left[\frac{B}{A}\right]^2 e^{3I_t+I_b} \tag{5.15}$$

with m_t determined from Fig. 1(a) and Eq. (4.8). Thus B/A actually depends on two inputs m_c and m_b, and on α_s. The ratio C/A is obtained by taking the determinant of the lepton Yukawa matrix of Eq. (5.14) and dividing by $\lambda_{t_G}^3$:

$$\frac{m_em_\mu}{m_\tau^2}=\frac{\eta_e\eta_\mu}{\eta_\tau^2}\left[\frac{C}{A}\right]^2 e^{6I_\tau}\ . \tag{5.16}$$

We are left with the determination of E and ϕ from m_μ and $\sin\theta_C$. Diagonalization of the heavy 2×2 sectors of the **D** and **E** matrices gives

$$\left[\frac{\lambda_\mu}{\lambda_\tau}\right]_G=3\frac{E}{A}\sqrt{1-2\delta_e\cos\tilde{\phi}+\delta_e^2}\ , \tag{5.17a}$$

$$\left[\frac{\lambda_s}{\lambda_b}\right]_G=\frac{E}{A}\sqrt{1-2\delta_d\cos\tilde{\phi}+\delta_d^2}$$

$$\simeq\frac{E}{A}(1-\delta_d\cos\tilde{\phi})\ , \tag{5.17b}$$

[5] We have specifically allowed for the possibility $v_{10}>v_5$ in order to obtain models with $\chi<1$.

where the last step involves the approximation $|\delta_d| \ll 1$, valid in all 9 of our models. Here

$$\delta_e = \frac{x_e x_e'}{3}\frac{B^2}{AE} , \tag{5.18a}$$

$$\delta_d = x_d x_d' \frac{B^2}{AE} . \tag{5.18b}$$

Scaling (5.17a) to low energies gives

$$\frac{m_\mu}{m_\tau} = 3\left|\frac{E}{A}\right|\sqrt{1-2\delta_e\cos\tilde{\phi}+\delta_e^2}\,\frac{\eta_\mu}{\eta_\tau}e^{3I_\tau} , \tag{5.19}$$

which provides one equation for E and $\tilde{\phi}$.

The phase $\tilde{\phi}$ of the Yukawa matrices differs in general from the phase ϕ of the Cabibbo-KM (CKM) matrix. In the "22" texture $\phi = \phi_u - \phi_d = -\phi_d$ and the difference between $\tilde{\phi}$ and ϕ_d is small: $\tilde{\phi} - \phi_d \approx \delta_d$. In all nine models of interest δ_d is less than 0.1, and in most less than 0.01, hence in the rest of this section we take $\tilde{\phi} = -\phi$. A relation to determine ϕ follows from

$$\sin\theta_C = |V_{us}| = |s_1 + c_1 s_2 e^{-i\phi}| \tag{5.20}$$

so that ϕ is determined from

$$\cos\phi = \frac{\sin^2\theta_C - s_1^2 - s_2^2}{2s_1 s_2} , \tag{5.21}$$

where the angles θ_1 and θ_2 are given by

$$\tan\theta_1 = \frac{C}{\lambda_{s_G}} \simeq \frac{C}{E}(1+\delta_d\cos\phi) , \tag{5.22}$$

$$s_2 = \frac{C}{27\lambda_{c_G}} \simeq -\frac{1}{27 x_u x_u'}\frac{AC}{B^2} . \tag{5.23}$$

The ratios B/A, C/A, and E/A necessary to evaluate s_1 and s_2 are obtained from (5.15), (5.16), and (5.19). The sign of B/A has been chosen to make $s_3 > 0$, and we now choose the sign of C/A and E/A to make s_1 and s_2 positive. Thus, without loss of generality, the angles θ_1, θ_2, and θ_3 are all taken to lie in the first quadrant. Hence we have

$$\tan\theta_1 \simeq 3\left[\frac{m_e}{m_\mu}\right]^{1/2}\left[\frac{\eta_\mu}{\eta_e}\right]^{1/2}(1-\delta\cos\phi) , \tag{5.24}$$

where we have defined δ by

$$1-\delta\cos\phi \equiv \sqrt{1-2\delta_e\cos\phi+\delta_e^2}\,(1+\delta_d\cos\phi) . \tag{5.25}$$

In most of our models $|\delta_e| \ll 1$, in which case $\delta \simeq \delta_e - \delta_d$. Equation (5.24) is alternatively written as

$$s_1 \simeq 0.196(1-\delta\cos\phi) . \tag{5.26}$$

Inserting B/A and E/A into (5.18a) gives

$$\delta_e = -\frac{x_e x_e'}{x_u x_u'}\sqrt{1-2\delta_e\cos\phi+\delta_e^2}\,\frac{m_\tau}{m_\mu}\frac{m_c}{m_t}\frac{\eta_\mu}{\eta_\tau\eta_c} \times e^{-3I_t - I_b + 3I_\tau} \tag{5.27a}$$

and

$$\delta_d = \frac{3x_d x_d'}{x_e x_e'}\delta_e . \tag{5.27b}$$

The signs of δ_e and δ_d will be crucial: in (5.27) it is understood that θ_1 and θ_2 have been chosen in the first quadrant. Finally, using the determined values for C/A and B/A in (5.23) gives

$$s_2 = \frac{1}{27}\frac{m_e^{1/2} m_\mu^{1/2} m_t}{m_\tau m_c}\frac{\eta_c\eta_\tau}{\eta_e^{1/2}\eta_\mu^{1/2}}e^{3I_t + I_b - 3I_\tau} . \tag{5.28}$$

The analytic determination of $\cos\phi$ in a particular model is not completely straightforward. This is because $\cos\phi$ occurs in both (5.26) and (5.27a) so Eq. (5.21) becomes a polynomial of high order in $\cos\phi$. The analysis simplifies considerably for the models with $|\delta_e| \ll 1$, since then the square root factor in (5.27a) may be neglected in estimating δ_e.

This concludes the parameter determination: A from m_b/m_τ via (4.10); $\tan\beta$ from m_τ via (4.11); B/A from m_c/m_τ via (5.15); C/A from $m_e m_\mu/m_\tau^2$ via (5.16); E/A from m_μ/m_τ via (5.19); ϕ from $\sin\theta_C$ via (5.21).

Before proceeding to the eight predictions, we show why the predictions for m_s/m_d disfavors some of the nine models. From the determinant of **D** and **E** we find

$$\frac{m_s}{m_d}\left[1-\frac{m_d}{m_s}\right]^2 = \frac{1}{9}\frac{m_\mu}{m_e}\left[1-\frac{m_e}{m_\mu}\right]^2\frac{\eta_\mu}{\eta_e}\frac{1}{(1-\delta\cos\phi)^2} , \tag{5.29}$$

where $1-\delta\cos\phi$ is given in (5.25). This reproduces one of the predictions of Georgi and Jarlskog [4] in the limit that $\delta_{e,d} \to 0$: $m_s/m_d = 25.15$. Since this is a high value for m_s/m_d, a very interesting feature of the present models is that this number is modified by $\delta_{e,d}$. We consider models with m_s/m_d larger than 25.15 to be disfavored. In general, the deviation of m_s/m_d from 25.15 will depend on the numerical value of the inputs m_c, m_b, and α_s. This dependence, and the quantitative value of m_s/m_d will be discussed in Sec. VI. However, the qualitative behavior of m_s/m_d can be understood from our analytic formulas.

To understand the qualitative deviation of m_s/m_d, the crucial question is the signs of δ and $\cos\phi$ for the nine models. The signs of δ_e and δ_d are determined by the signs of $x_e x_e'/x_u x_u'$ and $x_d x_d'/x_u x_u'$ which are listed in Table II.

Using (5.29), one can rewrite (5.27a) approximately as

$$\delta_e \simeq -0.043\frac{x_e x_e'}{x_u x_u'}\frac{m_c}{1.27\text{ GeV}}\frac{180\text{ GeV}}{m_t}\left[\frac{23}{m_s/m_d}\right]^{1/2} \times (1\mp 0.05) \tag{5.30}$$

for $\alpha_s(M_Z) = 0.115 \pm 0.005$. Thus, for many models, $|\delta_e|$ and $|\delta_d|$ are much less than unity, in which case δ appearing in (5.29) is given by $\delta \simeq \delta_e - \delta_d$. The sign of δ is then given by the sign of

$$c = \frac{3x_d x_d' - x_e x_e'}{x_u x_u'} ,$$

TABLE II. Useful combinations of Clebsch factors for the nine models.

	1	2	3	4	5	6	7	8	9
$\frac{x_e x_e'}{x_u x_u'}$	-1.5	-13.5	$\frac{1}{2}$	4.5	-6.75	2.25	$\frac{1}{9}$	1	9
$\frac{x_d x_d'}{x_u x_u'}$	$\frac{1}{6}$	$\frac{1}{6}$	$-\frac{1}{18}$	$-\frac{1}{18}$	$-\frac{1}{12}$	$\frac{1}{36}$	$\frac{1}{9}$	$\frac{1}{9}$	$\frac{1}{9}$
$c=\frac{3x_d x_d'-x_e x_e'}{x_u x_u'}$	2	14	$-\frac{2}{3}$	-4.7	6.5	-2.2	$\frac{2}{9}$	$-\frac{2}{3}$	-8.7
m_s/m_d	26.7	D	24.8	23.6	D	24.2	25.3	24.8	
χ	$\frac{2}{3}$	$\frac{2}{3}$	$\frac{2}{3}$	$\frac{2}{3}$	$\frac{5}{6}$	$\frac{5}{6}$	$\frac{8}{9}$	$\frac{8}{9}$	$\frac{8}{9}$
$\cos\phi$	0.35		0.24	0.16		0.20	0.27	0.24	
$\sin\phi$	0.94		0.97	0.99		0.98	0.96	0.97	

which is also listed in Table II. Consider the models with δ positive: if $\cos\phi$ is also positive m_s/m_d will be increased above 25.15 and the models disfavored. For models 1 and 7, $\delta_{e,d} \ll 1$ and $\delta \simeq \delta_e - \delta_d$ is positive. Because $\delta \ll 1$, (5.21) determines $\cos\phi$ to be positive: these two models do indeed give values of m_s/m_d larger than 25.15. The values of m_s/m_d, as well as $\cos\phi$ and $\sin\phi$ are shown in the table for $\alpha_s(M_Z)=0.115$. Note that for the models where c is not large, Eq. (5.21) can be approximated as $\cos\phi \simeq 0.26/(1-0.13c)$; where we have used $\alpha_s(M_Z)=0.115$ and $m_t=180$ GeV.

The other two models with

$$c=\frac{3x_d x_d - x_e x_e'}{x_u x_u'} > 0$$

are models 2 and 5. In these cases $|\delta_e|$ is not much less than unity, so the analysis is more complicated. However, it can be shown that $s_1 > 0.196$ (necessary for $m_s/m_d < 25.15$) can only occur for a very narrow range of δ_e near 0.40. Using Eq. (5.30) the central values of δ_e for models 2 and 5 are 0.59 and 0.30. To obtain an acceptable solution with δ_e near 0.40, parameters must be chosen far from their central values. While not excluded, we find these two models to be highly disfavored: in Table II we write "D" for disfavored. However, if extreme values of α_s are used in these theories, m_s/m_d can vary over the entire acceptable range.

Models 3, 6, and 8 all have $|\delta_e| \ll 1$ so that $\delta \simeq \delta_e - \delta_d$ and is negative. Furthermore, since $\cos\phi$ is positive for these three models, m_s/m_d is reduced slightly below 25.15. For models 4 and 9, the small $|\delta_e|$ approximation is no longer valid; nevertheless, one finds that in these models m_s/m_d is decreased even further, so that, from the viewpoint of m_s/m_d, these are the preferred models. However, in comparing with data it is important to study predictions for m_u/m_d simultaneously with m_s/m_d, and this will be done in the next section. From the numerical results of Fig. 5 one can see that m_s/m_d decreases in the sequence of models: 3 and 8, 6, 4, 9. This can be understood as successively larger deviations from the Georgi-Jarlskog result due to the Clebsch factor

$$c=\frac{3x_d x_d' - x_e x_e'}{x_u x_u'}$$

shown in Table II.

We now give analytic formulas for the eight predictions. The top mass m_t and β can be predicted from the analysis of the heaviest generation. With A and therefore I_i determined from (4.10),

$$\cos\beta = \frac{\sqrt{2} m_\tau}{av \prod_a \zeta_a^e \eta_\tau} e^{3I_b + 4I_\tau}, \tag{5.31}$$

$$m_t = \prod_a \left[\frac{\zeta_a^u}{\zeta_a^e}\right] \tan\beta \; m_\tau e^{-6I_t + 2I_b + 4I_\tau}. \tag{5.32}$$

RG scaling (5.9) to low energies gives

$$V_{cb} = \chi \left[\frac{m_c}{m_t}\right]^{1/2} \frac{1}{\sqrt{\eta_c}} e^{(I_b - I_t)/2}, \tag{5.33}$$

where χ is given in (5.10). This result illustrates how our predictions have the form:

$$\begin{bmatrix}\text{Predicted}\\ \text{Quantity}\end{bmatrix} = \begin{bmatrix}\text{GUT}\\ \text{Clebsch}\end{bmatrix} \begin{bmatrix}\text{Input}\\ \text{Quantity}\end{bmatrix} \begin{bmatrix}\text{RG}\\ \text{factor}\end{bmatrix}.$$

The strange mass is obtained from (5.17b):

$$m_s \simeq \frac{1}{3} m_b \frac{m_\mu}{m_\tau} \frac{1}{1-\delta\cos\phi} \frac{\eta_s}{\eta_b} \frac{\eta_\tau}{\eta_\mu} e^{3I_b + I_t - 3I_\tau}, \tag{5.34}$$

which can be simplified using (4.11) for m_b/m_τ. The prediction for m_s/m_d follows from the determinant of **D** and **E** and is given in (5.29). The prediction for m_u/m_d follows from the determinantal relation (4.13) with m_s from (5.34):

$$\frac{m_u}{m_d} \simeq \frac{1}{3^7} \frac{m_\mu}{m_\tau} \frac{m_t^2}{m_c m_b} \frac{1}{1-\delta\cos\phi} \eta_b \eta_c \frac{\eta_\tau}{\eta_\mu} e^{5I_t - I_b - 3I_\tau}. \tag{5.35}$$

From the form of the KM matrix of Eq. (4.3) one finds $V_{ub}/V_{cb} = s_2$, and using (5.28) this immediately gives

$$\frac{V_{ub}}{V_{cb}} \simeq \frac{1}{27} \frac{m_e^{1/2} m_\mu^{1/2}}{m_\tau} \frac{m_t}{m_c} \frac{\eta_c \eta_\tau}{\eta_e^{1/2} \eta_\mu^{1/2}} e^{3I_t + I_b - 3I_\tau}. \tag{5.36}$$

The final prediction is for the amount of CP violation in the KM matrix, which we choose to specify via the rephase invariant quantity J [21]:

$$J \equiv \mathrm{Im} V_{ud} V_{tb} V_{td}^* V_{ub}^* \simeq s_1 s_2 s_3^2 s_\phi$$
$$\simeq \frac{\chi^2}{9}\frac{m_e}{m_\tau}(1-\delta\cos\phi)s_\phi \frac{\eta_\tau}{\eta_e} e^{2I_t+2I_b-3I_\tau}, \quad (5.37)$$

where ϕ is obtained from (5.21). Since s_ϕ is determined to be near unity, the value of J can be obtained to within a factor of 2 from

$$J \simeq \frac{\chi^2}{9}\frac{m_e}{m_\tau} \simeq 3\times 10^{-5}\chi^2 .$$

In summary, our eight predictions for β, m_t, V_{cb}, m_s, m_s/m_d, m_u/m_d, V_{ub}/V_{cb}, and J are given in (5.29) and (5.31)–(5.37). An interesting feature of these predictions is that, of the six Clebsch factors which appear in the Yukawa matrices (x_u, x_u', x_d, x_d', x_e, and x_e'), only three linear combinations occur in physical observables:

$$\chi = |x_u - x_d|/\sqrt{|x_u x_u'|}$$

and $x_e x_e'/x_u x_u'$ and $x_d x_d'/x_u x_u'$ which occur in δ_e and δ_d. The combination χ occurs in the V_{cb} prediction and we have already seen that this limits us to consider only theories with $\chi = \frac{2}{3}, \frac{5}{6}$, and $\frac{8}{9}$.

In comparing the nine models, it is useful to recall that the m_t and $\tan\beta$ predictions are essentially universal. The distinctions between the models appear in the other predictions, which we now evaluate for inputs of $m_b = 4.25$ GeV, $m_c = 1.27$ GeV and $\alpha_s(M_Z) = 0.115 \pm 0.005$. In this case we find

$$V_{cb} \simeq 0.059\chi \left[\frac{180\text{ GeV}}{m_t}\right]^{1/2}(1\mp.03), \quad (5.38)$$

$$\frac{V_{ub}}{V_{cb}} \simeq 0.063\frac{m_t}{180\text{ GeV}}(1\pm 0.1), \quad (5.39)$$

where the range corresponds to $\alpha_s(M_Z) = 0.115 \pm 0.005$. Note that the predicted values for the running mass $m_t = m_t(m_t)$ should be used in these equations and in the remainder of this section. For the relevant m_b and α_s the predicted top pole mass, M_t, should be read from Fig. 1(a), and converted to the running mass using Eq. (4.8).

Predictions for m_s, m_u/m_d, and J can be obtained from Eqs. (5.34), (5.35), and (5.37):

$$m_s \simeq (168\pm 19)\left[\frac{m_s/m_d}{23}\right]^{1/2}\text{MeV}, \quad (5.40)$$

$$\frac{m_u}{m_d} \simeq 0.71\left[\frac{m_t}{180\text{ GeV}}\right]^2\left[\frac{m_s/m_d}{23}\right]^{1/2}(1\pm 0.13), \quad (5.41)$$

$$J \simeq 4.6\times 10^{-5}\chi^2\left[\frac{23}{m_s/m_d}\right]^{1/2}\sin\phi(1\pm 0.03) \quad (5.42)$$

for $\alpha_s(M_Z) = 0.115 \pm 0.005$. Note that Eq. (5.29) has been used to express $(1-\delta\cos\phi)$ in terms of m_s/m_d. From Table II it can be seen that $\sin\phi \simeq 1$.

Finally, we give approximate formulas for *CP* violation in K and B meson processes, and for $B^0\bar{B}^0$ mixing. Using the same central values as above, we find the kaon *CP* impurity parameter ϵ is given by

$$|\epsilon| \simeq 2.26\times 10^{-3}\left[\frac{\hat{B}_K}{0.51}\right]\left[\frac{\chi}{5/6}\right]^4\left[\frac{23}{m_s/m_d}\right]^{3/2}$$
$$\times\left[\frac{m_t}{180\text{ GeV}}\right]^{1/2}(1\mp 0.03) \quad (5.43)$$

for $\alpha_s(M_Z) = 0.115 \pm 0.005$. A lattice calculation gives $\hat{B}_K = 0.72 \pm 0.06$ [22], where the error includes only the uncertainty due to the continuum extrapolation. Other calculational approximations, such as the quenched approximation, lead to additional uncertainties. For $B_d^0\bar{B}_d^0$ mixing we find

$$x_d \equiv \frac{\Delta m}{\Gamma} \simeq 0.67\frac{\tau_B}{1.28\text{ ps}}\left[\frac{\sqrt{B}f_B}{175\text{ MeV}}\right]^2\left[\frac{\chi}{5/6}\right]^2$$
$$\times\frac{23}{m_s/m_d}\left[\frac{m_t}{180\text{ GeV}}\right]^{1/2}(1\mp 0.06) \quad (5.44)$$

showing that large χ prefers smaller f_B (which is normalized such that $f_\pi = 135$ MeV).

The *CP*-violating parameters $\sin 2\alpha$ and $\sin 2\beta$ measured in $B^0 \to \pi^+\pi^-$ and $B^0 \to \psi K_s$ are given in our models by

$$\sin 2\alpha = -2\cos\phi\sin\phi, \quad (5.45a)$$

$$\sin 2\beta = \frac{2c_1 s_1 s_2}{s_c^2}\sin\phi\left[1+\frac{c_1 s_2}{s_1}\cos\phi\right]. \quad (5.45b)$$

From Table II it can be seen that the six models where c is not large have $|\cos\phi| < 0.35$. In this case, the factor $(c_1 s_2/s_1)\cos\phi$ is less than 0.1 and can be neglected in (5.45b). Since these models all have $\sin\phi \simeq 1$, we find $\sin 2\beta = 2s_1 s_2/s_c^2$. Using s_1 from Eq. (5.26) and $s_2 \simeq 0.063(1\pm 0.1)$ we find that these models all lead to essentially the same β:

$$\sin 2\beta \simeq 0.54\left[\frac{23}{m_s/m_d}\right]^{1/2}(1\pm 0.15). \quad (5.46a)$$

On the other hand, these six models do have variation in $\cos\phi$, as shown in Table II, so they can be distinguished by $\sin 2\alpha$:

$$\sin 2\alpha \simeq -(0.66,\ 0.47,\ 0.32,\ 0.40,\ 0.52,\ 0.47) \quad (5.46b)$$

for models 1, 3, 4, 6, 7, and 8, respectively.

These numbers, and the predictions of Table II, are for $\alpha_s(M_Z) = 0.115$ and $m_t = 180$ GeV. The full predictions for these models, and also for models 2, 5, and 9, where c is large, will be given in the next section. In Appendix D we show that the predictions of this section survive, with certain modifications, even if there are large supersymmetric threshold corrections to λ_b which give a lighter top quark. In Appendix E we discuss the extent to which these predictions are affected by GUT threshold corrections, including relaxation of the assumption that both Higgs doublets lie in a single **10**.

VI. A QUANTITATIVE STUDY OF THE "22" TEXTURE

In this section we present a quantitative analysis of the eight predictions in each of the models with "22" texture. To obtain the numbers quoted in this section we numerically integrated the full two-loop renormalization-group equations from the grand unification scale down to the weak scale. At the grand unified scale, a small threshold correction was applied to the strong-coupling constant in order to obtain a prescribed value of $\alpha_s(M_Z)$. At the weak scale, one-loop matching corrections were applied to account for a degenerate spectrum of superpartners. For definiteness sake, we show our predictions for $M_{\rm SUSY}=M_{\rm weak}=180$ GeV; however, we have varied both these scales separately and our results do not change by more than a few percent. At the weak scale, the Yukawa couplings were diagonalized and the mixing angles were determined. The fermion masses obtained at the weak scale were subsequently evolved to three loops in QCD and two loops in QED from the weak scale down to the larger of either the particles mass or 1 GeV.

In addition to the numerical evolution described above, we have performed a numerical search to discover all possible models having the "22" texture. Using the uniquely viable operators O_{12} and O_{33} discussed in Sec. IV, we searched through all possible pairings of operators O_{22} and O_{23} up to dimension 6. In this search, we demanded $m_s=199\pm66$ MeV, $0.5<\chi<1$, where $V_{cb}=\chi\sqrt{m_c/m_t}$, $0.03<V_{ub}/V_{cb}<0.1$, $17<m_s/m_d<26$, and $0.2<m_u/m_d<0.7$. All of the models which passed these constraints simultaneously had a "22" operator with a 0:1:3 Clebsch factor, thus establishing the uniqueness of the O_{22} operators in Eq. (5.6). Furthermore, the search resulted in nine acceptable "23" operators, which are precisely those given in Eq. (5.12), and we now turn to the predictions of these nine different "22" models.

Because the large hierarchy within the third generation is explained by the dynamical factor $\tan\beta$, and because an acceptable m_b/m_τ requires a top quark Yukawa coupling of order unity, the top quark mass and $\tan\beta$ are predicted to be large. As shown in Fig. 1, 166 GeV $<M_t<$ 192 GeV, and $51<\tan\beta<63$. The predictions for the top quark mass and $\tan\beta$ shown in Fig. 1, arise when all three third generation Yukawa couplings are equal at the grand unification scale. Perturbative corrections to this equality occur when the operator O_{23} has large Clebsch factors since the third generation Yukawa couplings are equal to

$$\lambda_i^2=A^2+(x_i^2+x_i'^2)B^2 \tag{6.1}$$

at the unification scale. This effect is numerically insignificant in most models, because typically $x_iB/A\approx V_{cb}$. However, V_{cb} actually constrains only $(x_d-x_u)B/A$, and occasionally some x_i and x_i' Clebsch factors, particularly those with $i=e$, happen to be large. Of the nine models, this is most significant in model 9 where the top quark mass prediction is decreased by 5–10 GeV.

The nine "22" texture models separate into three groups according to their predictions for V_{cb}: $V_{cb}=\chi\sqrt{m_c/m_t}$ with $\chi=\frac{2}{3}, \frac{5}{6}, \frac{8}{9}$. These three classes of V_{cb} predictions are shown in Fig. 4 along with the prediction for $\chi=1$. The values of V_{cb} obtained from exclusive B decays using heavy quark effective theory favors the $\chi=\frac{2}{3}$ and $\frac{5}{6}$ models. Figure 4 also shows that the Harvey-Ramond-Reiss (HRR) [4] relation $V_{cb}=\sqrt{m_c/m_t}$ is incompatible with a framework which unifies the third generation Yukawa couplings because it leads to unacceptably large values of V_{cb}.

A second feature which distinguishes the nine models

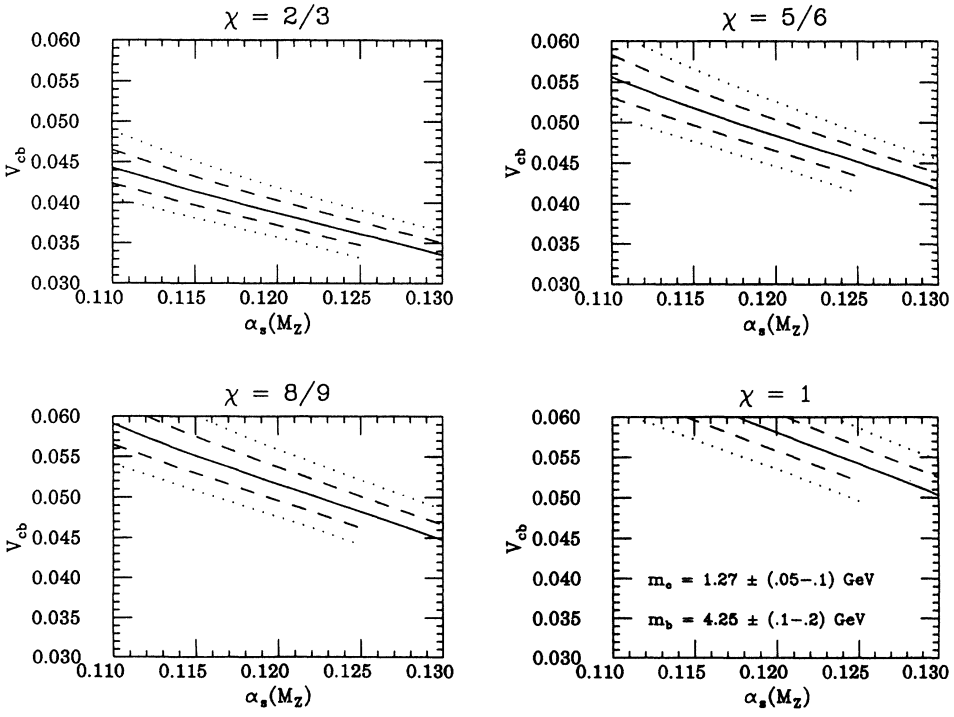

FIG. 4. $V_{cb}=\chi\sqrt{m_c/m_t}$ plotted as a function of $\alpha_s(M_Z)$ for $\chi=\frac{2}{3}, \frac{5}{6}, \frac{8}{9}$, and 1. The region between the dashed (dotted) curves is the range of predictions for V_{cb} for $m_c(m_c)=1.27\pm0.05(0.1)$ GeV and $m_b(m_b)=4.25\pm0.1(0.2)$ GeV. The solid curve gives the prediction for V_{cb} with central values of m_c and m_b. Some of the curves are not continuous across the figure because the GUT-scale Yukawa coupling becomes nonperturbative for small $m_b(m_b)$ and large α_s [see Fig. 1(a)].

is the predictions for m_s/m_d. We can compare these predictions to the chiral perturbation theory determination of light quark mass ratios. Second-order chiral perturbation theory along with Dashen's theorem can be used to determine the light quark mass ratios m_s/m_d and m_u/m_d in terms of the pseudoscalar meson masses [23,24]:

$$\frac{1}{Q^2}\left[\frac{m_s}{m_d}\right]^2+\left[\frac{m_u}{m_d}\right]^2=1\ , \tag{6.2a}$$

where

$$Q^2=\frac{M_K^2}{M_\pi^2}\frac{M_K^2-M_\pi^2}{M_{K^0}^2-M_{K^+}^2+M_{\pi^+}^2-M_{\pi^0}^2}\simeq 24^2\ . \tag{6.2b}$$

The theoretical uncertainties in Eq. (6.2) can be cast as an uncertainty in Q. Figures 5(a), 5(b), and 5(c) compare the light quark mass ratio predictions of the nine "22" models. When the inputs are restricted to the ranges $m_b(m_b)=4.25\pm0.1$ GeV, $m_c(m_c)=1.27\pm0.05$ GeV, and $\alpha_s(M_Z)=0.120\pm0.01$, only models 2, 4, 6, and 9 can yield successful predictions with models 4, 6, and 9 providing the most successful predictions. The prediction of the light quark mass ratios gives a preference for low values for $\alpha_s(M_Z)$ in all models.

As discussed at the end of this section, the $\chi=\frac{2}{3}$ models do not have enough *CP* violation to explain the kaon *CP* impurity parameter ϵ. So the requirement that these models account for the observed *CP* violation eliminates models 1–4, leaving us with two remaining candidates: 6

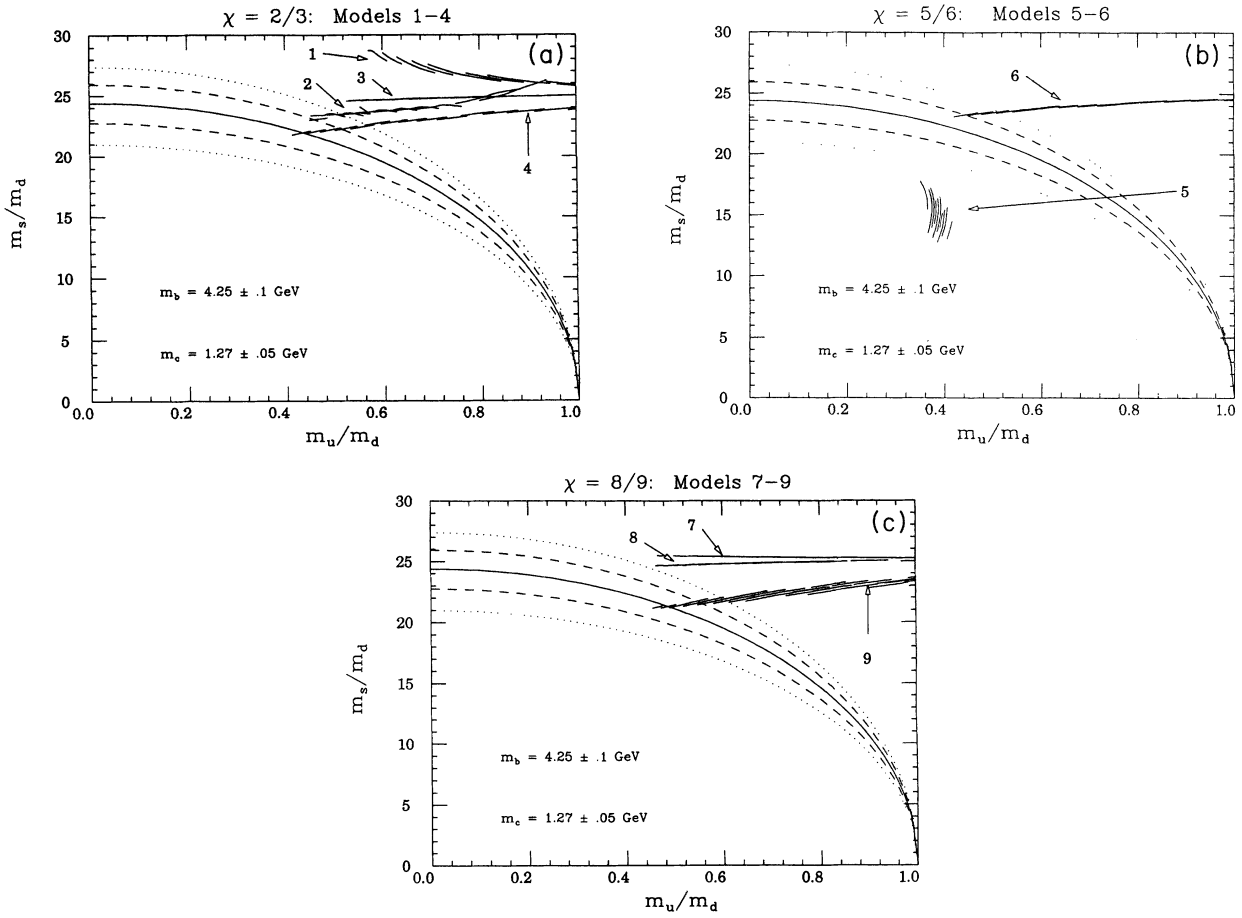

FIG. 5. (a) Light quark mass ratios for the $\chi=\frac{2}{3}$ models. The mass ratio m_s/m_d is plotted as a function of m_u/m_d. These values are obtained for the range of inputs: $m_b(m_b)=4.25\pm0.1$, $m_c(m_c)=1.27\pm0.05$, and $\alpha_s(M_Z)=0.110$–0.125. The dependence of m_u/m_d on these input parameters can be obtained from equation 5.35, or, more accurately, from Figs. 6 and 7 for models 9 and 6, respectively. The quarter ellipse is the second-order chiral perturbation theory prediction for the light quark mass ratios of Eq. (6.2). The dashed (dotted) ellipses are obtained when the Q in Eq. (6.2) is assumed to be uncertain by 13% (26%). (b) Light quark mass ratios for the $\chi=\frac{5}{6}$ models. The mass ratio m_s/m_d is plotted as a function of m_u/m_d. These values are obtained for the range of inputs: $m_b(m_b)=4.25\pm0.1$, $m_c(m_c)=1.27\pm0.05$ and $\alpha_s(M_Z)=0.110-125$. The dependence of m_u/m_d on these input parameters can be obtained from equation 5.35, or, more accurately, from Figs. 6 and 7 for models 9 and 6, respectively. The quarter ellipse is the second-order chiral perturbation theory prediction for the light quark mass ratios of Eq. (6.2). The dashed (dotted) ellipses are obtained when the Q in Eq. (6.2) is assumed to be uncertain by 13% (26%). (c) Light quark mass ratios for the $\chi=\frac{8}{9}$ models. The mass ratio m_s/m_d is plotted as a function of m_u/m_d. These values are obtained for the range of inputs: $m_b(m_b)=4.25\pm0.1$, $m_c(m_c)=1.27\pm0.05$, and $\alpha_s(M_Z)=0.110-125$. The quarter ellipse is the second-order chiral perturbation theory prediction for the light quark mass ratios of Eq. (6.2). The dashed (dotted) ellipses are obtained when the Q in Eq. (6.2) is assumed to be uncertain by 13% (26%).

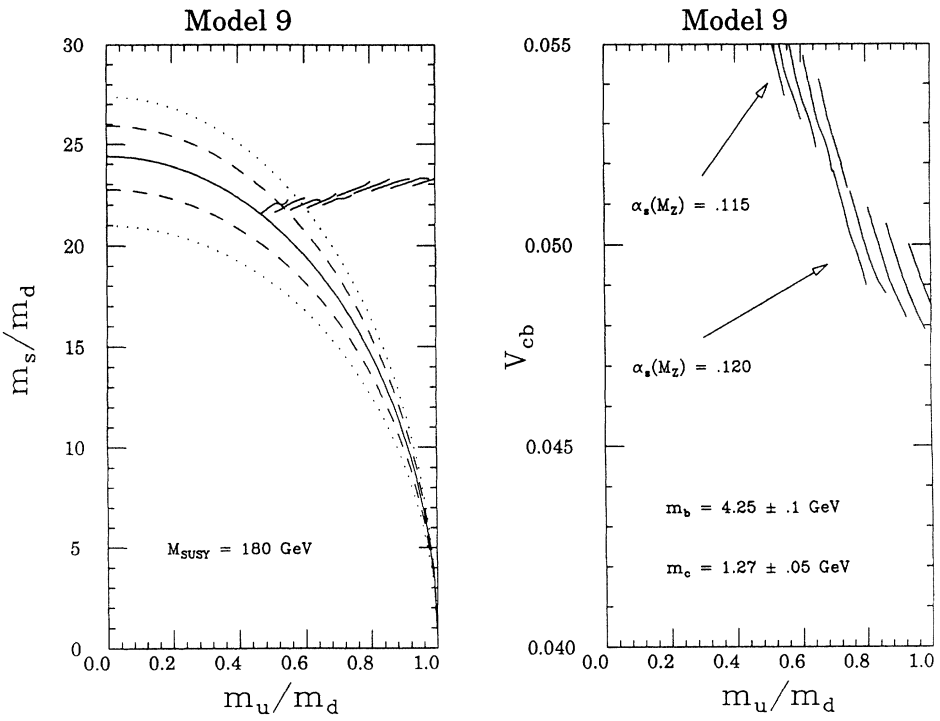

FIG. 6. m_s/m_d and V_{cb} are plotted as a function of m_u/m_d for model 9. The same set of inputs has been used in both figures: $m_b(m_b)=4.25\pm0.1$, $m_c(m_c)=1.27\pm0.05$, and $\alpha_s(M_Z)=0.110$, 0.115, 0.120. For each value of $\alpha_s(M_Z)$ the prediction is given by five solid lines, each of which corresponds to a definite value of $m_b(m_b)$, which steps by 0.05 GeV between lines. Along each line the input value of $m_c(m_c)$ is varied. The predicted value for m_u/m_d decreases as either $m_b(m_b)$ or $m_c(m_c)$ is increased.

and 9. As an important discriminator, we show that correlations between the predictions for V_{cb} and m_u/m_d tends to disfavor model 9. For all nine models, predictions for m_u/m_d small enough to agree well with the chiral perturbation theory determination occur for large values of the inputs $m_b(m_b)$ and $m_c(m_c)$, and small values of $\alpha_s(M_Z)$. Each of these leads to a larger value of V_{cb}. For example, with model 9 $m_u/m_d<0.6$ requires $V_{cb}>0.052$. This competition is shown in Figs. 6 and 7 for models 9 and 6, respectively. It may be over zealous to say that model 9 is ruled out by this analysis because there are uncertainties in these calculations at the level of a few percent, and we have used a conservative range of inputs in this analysis. However, the empirical value of fermion masses and mixing angles seems to show a preference for model 6.

At the level where they can be probed experimentally, the predictions for m_s and V_{ub}/V_{cb} are fairly universal

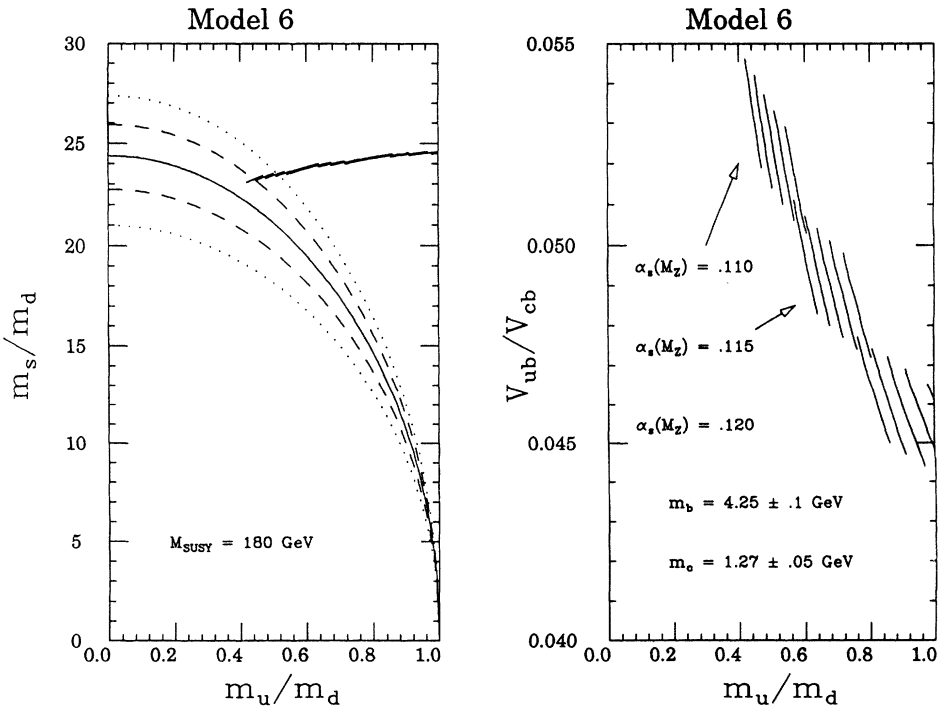

FIG. 7. m_s/m_d and V_{cb} are plotted as a function of m_u/m_d for model 6. The same set of inputs has been used in both figures: $m_b(m_b)=4.25\pm0.1$, $m_c(m_c)=1.27\pm0.05$ and $\alpha_s(M_Z)=0.115$, 0.120. For each value of $\alpha_s(M_Z)$ the prediction is given by five solid lines, each of which corresponds to a definite value of $m_b(m_b)$, which steps by 0.05 GeV between lines. Along each line the input value of $m_c(m_c)$ is varied. The predicted value for m_u/m_d decreases as either $m_b(m_b)$ or $m_c(m_c)$ is increased.

between the nine "22" models. For the sake of definiteness, the model 6 predictions are shown in Figs. 8 and 9. Both predictions are in excellent agreement with current determinations. The successful prediction for the strange quark mass reflects the Georgi-Jarlskog factor of 3, which is incorporated in the operator O_{22}.

The final prediction for these models is for ϵ, the measure of *CP* impurity in K_L and K_S. The dominant contribution to ϵ comes from the standard model box diagram amplitude, which may be written as a function of CKM elements and quark masses multiplied by a QCD matrix element B_K [27]. Using this result, together with the measured value of ϵ and our predictions for quark masses and CKM parameters, we can give a prediction for the matrix element B_K. In the theoretical formula for ϵ [28] we use input quantities renormalized at μ such that $\alpha_s(\mu)=1$, hence the predicted quantity is $\hat{B}_K$. Figure 10 shows the range of predictions for $\hat{B}_K$ for the nine "22" models. Five of the nine models predict values of $\hat{B}_K$ that agree well with the lattice determination of $\hat{B}_K=0.72\pm0.06$ [22], where the error includes only the uncertainty due to the continuum extrapolation. Other calculational approximations, such as the quenched approximation, lead to additional uncertainties. The $\chi=\frac{2}{3}$ models give insufficient *CP* violation, and can be excluded if we demand that the observed *CP* violation in the kaon system arise from the *CP*-violating phase in the CKM matrix.

Predictions for $\sin2\alpha$ and $\sin2\beta$ provide a complimentary method of distinguishing and testing the nine "22" models. Most importantly, measurements of these angles from *CP*-violating asymmetries in *B* decays provide a potentially more stringent test of these models. Figures 11(a)–11(c) display the $\sin2\alpha$ vs $\sin2\beta$ predictions of models 1–9. Also shown is the expected size of the experimental error bar for an integrated luminosity of 10^{41} cm^{-2} at an asymmetric *B* factory. Such measurements could exclude our entire scheme. They could also distinguish between some (e.g., 5 and 6) but not all (e.g., 7 and 8) models.

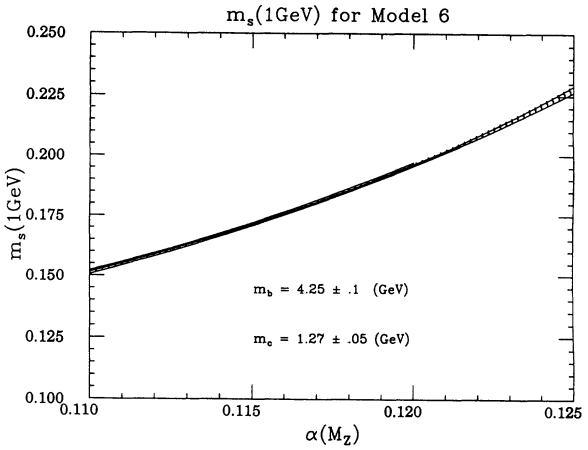

FIG. 9. The strange quark mass predictions is plotted as a function of $\alpha_s(M_Z)$ for model 6.

Finally, we provide three examples of particular predictions to demonstrate the degree of simultaneous success each class of model can achieve. In addition to these predictions, the set of inputs in Table III predicts

$$\sin2\alpha=-0.32,\quad \sin2\beta=0.39,\quad \sin2\gamma=0.66\ ,$$

and

$$J=1.75\times10^{-5}\ .$$

In addition to these predictions, the set of inputs in Table IV predicts

$$\sin2\alpha=-0.46,\quad \sin2\beta=0.49,\quad \sin2\gamma=0.84\ ,$$

and

$$J=2.6\times10^{-5}\ .$$

In addition to these predictions, the set of inputs in Table V predicts

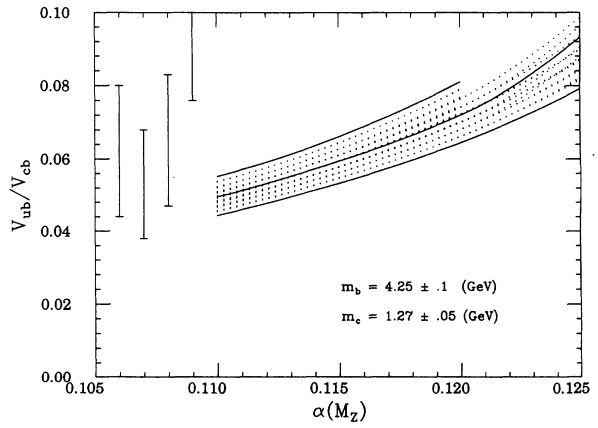

FIG. 8. V_{ub}/V_{cb} is plotted as a function of $\alpha_s(M_Z)$ in model 6. The error bars at the left of the graph represent several determinations, together with the uncertainties, of V_{ub}/V_{cb} from 1992 CLEO data on the end-point spectrum of semileptonic *B* decays [26].

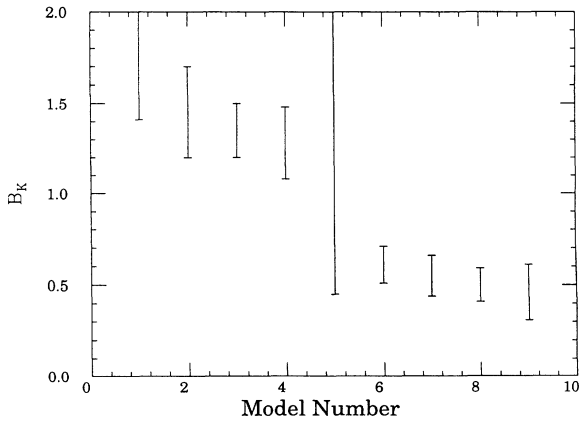

FIG. 10. The range of $\hat{B}_K$ predictions for models 1–9. The input quantities for this figure were evaluated at a scale μ where $\alpha_s(\mu)=1$. With the exception of the $\chi=\frac{2}{3}$ models, all these determinations agree well with the lattice estimates of roughly 0.6.

TABLE III. Particular predictions for model 4 with $\alpha_s(M_Z)=0.110$.

Input quantity	Input value	Predicted quantity	Predicted value
$m_b(m_b)$	4.35 GeV	M_t	166 GeV
$m_\tau(m_\tau)$	1.777 GeV	$\tan\beta$	51
$m_c(m_c)$	1.32 GeV	V_{cb}	0.043
m_μ	105.6 MeV	V_{ub}/V_{cb}	0.046
m_e	0.511 MeV	m_s (1 GeV)	147 MeV
V_{us}	0.221	$\hat{B}_K$	1.1
		m_u/m_d	0.41
		m_s/m_d	22.0

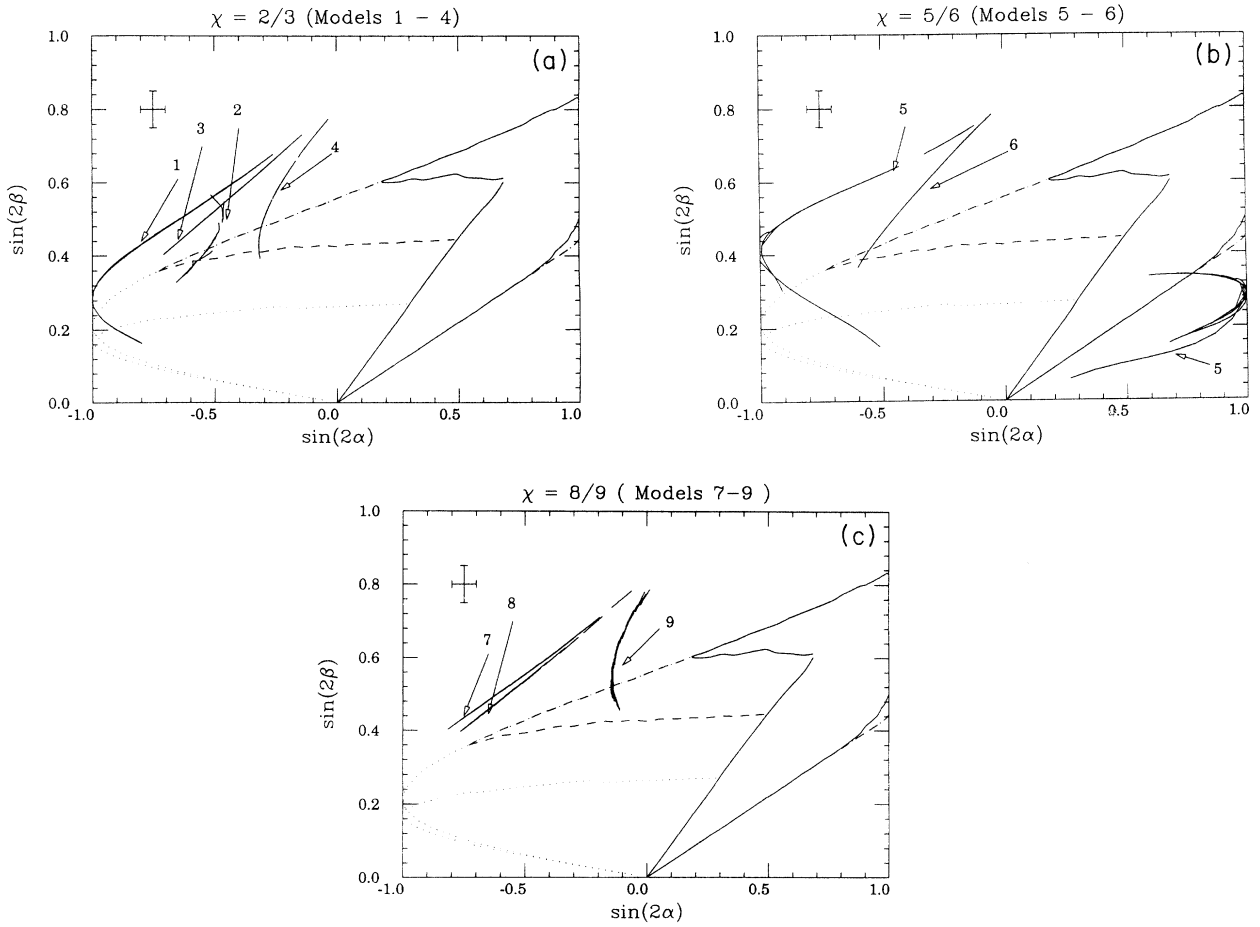

FIG. 11. (a) $\sin2\beta$ vs $\sin2\alpha$ for the $\chi=\frac{2}{3}$ models. Predictions for the four $\chi=\frac{2}{3}$ models are drawn over three different backgrounds representing allowed regions. The area inside the solid curve shows the allowed region for theories in which the GUT-scale Yukawa coupling matrices have vanishing (13), (31), and (11) entries, m_s/m_d and m_u/m_d lie between the dotted curves of Fig. 5, and $V_{ub}/V_{cb}>0.07$. If this lower bound on V_{ub}/V_{cb} is reduced to 0.05 (0.03), the background expands to the dashed (dotted) curve. The prediction for each model appears as a line, with larger values of $\sin2\beta$ corresponding to larger $\alpha_s(M_Z)$. (b) $\sin2\beta$ vs $\sin2\alpha$ for the $\chi=\frac{5}{6}$ models. Predictions for the two $\chi=\frac{5}{6}$ models are drawn over three different backgrounds representing allowed regions. The area inside the solid curve shows the allowed region for theories in which the GUT-scale Yukawa coupling matrices have vanishing (13), (31), and (11) entries, m_s/m_d and m_u/m_d lie between the dotted curves of Fig. 5, and $V_{ub}/V_{cb}>0.07$. If this lower bound on V_{ub}/V_{cb} is reduced to 0.05 (0.03), the background expands to the dashed (dotted) curve. The prediction for each model appears as a line, with larger values of $\sin2\beta$ corresponding to larger $\alpha_s(M_Z)$. (c) $\sin2\beta$ vs $\sin2\alpha$ for the $\chi=\frac{8}{9}$ models. Predictions for the three $\chi=\frac{8}{9}$ models are drawn over three different backgrounds representing allowed regions. The area inside the solid curve shows the allowed region for theories in which the GUT-scale Yukawa coupling matrices have vanishing (13), (31), and (11) entries, m_s/m_d and m_u/m_d lie between the dotted curves of Fig. 5, and $V_{ub}/V_{cb}>0.07$. If this lower bound on V_{ub}/V_{cb} is reduced to 0.05 (0.03), the background expands to the dashed (dotted) curve. The prediction for each model appears as a line, with larger values of $\sin2\beta$ corresponding to larger $\alpha_s(M_Z)$.

TABLE IV. Particular predictions for model 6 with $\alpha_s(M_Z)=0.115$.

Input quantity	Input value	Predicted quantity	Predicted value
$m_b(m_b)$	4.35 GeV	M_t	176 GeV
$m_\tau(m_\tau)$	1.777 GeV	$\tan\beta$	55
$m_c(m_c)$	1.22 GeV	V_{cb}	0.048
m_μ	105.6 MeV	V_{ub}/V_{cb}	0.059
m_e	0.511 MeV	m_s (1 GeV)	172 MeV
V_{us}	0.221	$\hat{B}_K$	0.64
		m_u/m_d	0.64
		m_s/m_d	24.0

$$\sin2\alpha=-0.14,\quad \sin2\beta=0.59,\quad \sin2\gamma=0.70\ ,$$

and

$$J=3.6\times10^{-5}\ .$$

VII. THE "23" TEXTURE

In this section we study the second GUT scale Yukawa texture which could arise from an SO(10) flavor sector with just four operators. The four operators of this "23" texture are shown in Eq. (3.2), and lead to Yukawa matrices which can be written in a form analogous to (5.1):

$$\lambda_i=\begin{bmatrix} 0 & z_i'C & 0 \\ z_iC & 0 & x_i'\exp(i\phi_i')B \\ 0 & x_i\exp(i\phi_i)B & A \end{bmatrix}, \tag{7.1}$$

where $i=u,d,e$,

$$x_i^{(\prime)}e^{i\phi_i^{(\prime)}}=x_{ia}^{(\prime)}+\gamma e^{i\phi}x_{ib}^{(\prime)} \tag{7.2}$$

is the complex linear combination of Clebsch factors arising from the operator $O_{23}=O_{23}^a+\gamma e^{i\phi}O_{23}^b$. [Strictly speaking, we should distinguish between the γ which appears in the linear combination of operators and the γ which appears in the linear combination of Clebsch factors contributing to the Yukawa entries. These γ's are actually related by a real multiplicative constant, because the Higgs vacuum expectation values which contribute to $O_{23}^{(a,b)}$ may be differently normalized. We absorb this factor into the definition of γ in (7.2).] For any given model, the values of $x_i^{(\prime)}$ (and $z_i^{(\prime)}$) can be obtained from Table I. By making phase rotations on the left and right matter multiplets, this form for λ_i can be brought into that of (5.1), $(\phi_i,\phi_i'=0)$ with $y_i=0$:

$$\lambda_i\rightarrow\begin{bmatrix} e^{i\phi_i} & 0 & 0 \\ 0 & e^{-i\phi_i'} & 0 \\ 0 & 0 & 1 \end{bmatrix}\lambda_i\begin{bmatrix} e^{i\phi_i'} & 0 & 0 \\ 0 & e^{-i\phi_i} & 0 \\ 0 & 0 & 1 \end{bmatrix}.$$

Approximate diagonal forms for these matrices at the GUT scale can then be obtained by essentially the same sequence of transformations as was used to diagonalize the matrices (5.1): (i) In the heavy 2×2 sector rotate the left-handed fermions by angles $\alpha_i=x_iB/A$ and the right-handed ones by $\alpha_i'=x_i'B/A$; (ii) write the resulting 22 entry as y_iE_i; (iii) diagonalize the light 2×2 sector by rotations $\beta_i=z_iC/y_iE_i$ and $\beta_i'=z_i'C/y_iE_i$ on the left- and right-handed fermions, respectively.

Let $\bar{\theta}_3=-\alpha_u$, $\bar{\theta}_4=-\alpha_d$, $\theta_2=-\beta_u$, $\theta_1=-\beta_d$, then the transformations in the left-handed up and down sector are

$$V_u=\begin{bmatrix} c_2 & s_2 & 0 \\ -s_2 & c_2 & 0 \\ 0 & 0 & 1 \end{bmatrix}\begin{bmatrix} 1 & 0 & 0 \\ 0 & \bar{c}_3 & \bar{s}_3 \\ 0 & -\bar{s}_3 & \bar{c}_3 \end{bmatrix}\begin{bmatrix} e^{-i\phi_u'} & 0 & 0 \\ 0 & e^{i\phi_u} & 0 \\ 0 & 0 & 1 \end{bmatrix}, \tag{7.3a}$$

TABLE V. Particular predictions for model 9 with $\alpha_s(M_Z)=0.120$.

Input quantity	Input value	Predicted quantity	Predicted value
$m_b(m_b)$	4.35 GeV	M_t	180 GeV
$m_\tau(m_\tau)$	1.777 GeV	$\tan\beta$	58
$m_c(m_c)$	1.27 GeV	V_{cb}	0.050
m_μ	105.6 MeV	V_{ub}/V_{cb}	0.071
m_e	0.511 MeV	m_s (1 GeV)	172 MeV
V_{us}	0.221	$\hat{B}_K$	0.43
		m_u/m_d	0.75
		m_s/m_d	23.0

$$V_d = \begin{pmatrix} c_1 & -s_1 & 0 \\ s_1 & c_1 & 0 \\ 0 & 0 & 1 \end{pmatrix} \begin{pmatrix} 1 & 0 & 0 \\ 0 & \bar{c}_4 & \bar{s}_4 \\ 0 & -\bar{s}_4 & \bar{c}_4 \end{pmatrix} \begin{pmatrix} e^{-i\phi_d'} & 0 & 0 \\ 0 & e^{i\phi_d} & 0 \\ 0 & 0 & 1 \end{pmatrix} . \tag{7.3b}$$

The resulting KM matrix, $V = V_u V_d^\dagger$, is not of the form (4.3) for general choices of ϕ_i, ϕ_i' (although one more phase redefinition can bring it into this form).

As discussed above and proved in Appendix C, once the 33 operator has been chosen the choice of the 12 operator is unique. It is only the choice of 23 operators which remains to determine the model. This selection is constrained primarily by the crucial relation (5.4e),

$$V_{cb_G}^2 \simeq \left| \frac{\lambda_c}{\lambda_t} \right|_G \ll \left| \frac{\lambda_\mu}{\lambda_\tau} \right|_G \simeq 3 \left| \frac{\lambda_s}{\lambda_b} \right|_G \tag{5.4e}$$

which indicates a division into two small parameters and two large ones. In the case of the "22" texture," the small parameters were obtained from the 23 operators, and the large ones from the 22 operators. Here, no such separation is possible; all four parameters are generated by the same linear combination of operators. The hierarchy must therefore result from a set of Clebsch factors which allow cancellations between the contributions from O_{23}^a and O_{23}^b to both V_{cb} and λ_c/λ_t, for similar values of $\gamma \exp[i\phi]$. This cancellation implies that the hierarchy of Eq. (5.4e) is unnatural, and it is for this reason that we prefer the "22" models to the "23" models.

Unfortunately, the complex nature of O_{23} in the 23 texture also makes these models considerably less amenable to analytic treatment than were the 22 models. The reason is clear. Whereas in the 22 models [Eq. (5.1)] the complex phase ϕ which appeared in the 22 entry of λ_i was the same for $i = u,d,e$, in the 23 models the one input phase ϕ appears as six distinct phases ϕ_i, ϕ_i' in the Yukawa matrices. The relation of these $\phi_i^{(\prime)}$ to ϕ is Clebsch dependent and hence depends on the particular model.

We have therefore undertaken a numerical search of all possible dimension-five and -six operators $O_{23}^{a,b}$ satisfying our dynamical hypotheses. (There are approximately 20 000 such operator pairs.) If any significant fraction of these models reproduced the available experimental data, then the probability of being able to make useful predictions from this approach would be small; for any realistically achievable experimental error bars, the predictions would likely be dense in the experimental plane. Fortunately, it is very likely that any individual model will work.

The search was performed by first considering the GUT-scale predictions for the quark and charged-lepton mass ratios and mixing angles, which [to leading order in the small quantities (B/A) and (C/A)] are

$$\frac{\lambda_s/\lambda_b}{\lambda_\mu/\lambda_\tau} = \frac{\lambda_s}{\lambda_\mu} = \frac{|x_d x_d'|}{|x_e x_e'|} , \tag{7.4a}$$

$$\frac{\lambda_c/\lambda_t}{\lambda_s/\lambda_b} = \frac{\lambda_c}{\lambda_s} = \frac{|x_u x_u'|}{|x_d x_d'|} , \tag{7.4b}$$

$$\frac{V_{cb}^2}{\lambda_c/\lambda_t} = \frac{|x_d e^{i\phi_d} - x_u e^{i\phi_u}|^2}{|x_u x_u'|} , \tag{7.4c}$$

$$\frac{\sin\theta_C}{\sqrt{\lambda_e/\lambda_\mu}} = \left| \frac{1}{x_d x_d' e^{i(\phi_d+\phi_d')}} + \frac{1/27}{x_u x_u' e^{i(\phi_u+\phi_u')}} \right| |x_e x_e'| . \tag{7.4d}$$

(The predictions for the first generation masses being fixed by the 12 operator.) Here all Yukawa couplings λ_a are evaluated at the GUT scale.

Although these expressions involve ratios of masses at the GUT scale, we understand their running well enough to be able to make some definitive statements. In particular, $(\lambda_e/\lambda_\mu) = (m_e/m_\mu)$ and $\sin\theta_C$ essentially do not run from the GUT scale down to low energies, so that $(\sin\theta_C/\sqrt{m_e/m_\mu})_G \simeq 0.015$, while, as discussed above [Eq. (5.4e)], $(\lambda_s/\lambda_\mu)_G = \frac{1}{3}$ in any theory where $\lambda_t = \lambda_b = \lambda_\tau$ at $M_{\rm GUT}$. Since $x_i^{(\prime)} e^{i\phi_i^{(\prime)}} = x_{ia}^{(\prime)} + \gamma e^{i\phi} x_{ib}^{(\prime)}$, Eqs. (7.2a) and (7.2d) determine $\gamma e^{i\phi}$. Unfortunately, they cannot be solved analytically for arbitrary values of $x_{ia}^{(\prime)}$ and $x_{ib}^{(\prime)}$. Therefore, for each possible choice of 23-operator pair, we solved Eqs. (7.2a) and (7.2d) numerically to find the allowed value(s) of γ and ϕ for a small range of input values about the central values given above. This range allows for experimental uncertainties, for any small amount of renormalization, and for the difference between the exact and leading-order eigenvalues of the λ^i and the rotations needed to diagonalize them. (The latter being particularly crucial for $\sin\theta_C$.) For each case we either obtained values for γ and ϕ or discovered that the equations have no solution. For those models for which values of γ and ϕ were obtained, Eqs. (7.2b) and (7.2c) were used to predict the GUT-scale values of (λ_c/λ_s) and $V_{cb}/\sqrt{(\lambda_c/\lambda_t)} \equiv \chi$. As shown above [Eqs. (5.4) and (5.11)], the allowed ranges for these quantities are $0.55 < \chi < 0.92$ and $0.085 \lesssim (\lambda_c/\lambda_s)_G \lesssim 0.19$.

Demanding that $(\lambda_c/\lambda_s)_G$ and χ lie within their allowed ranges, we were able to reduce the number of possible 23 models to less than 100. These we explored individually by running them down from the GUT scale to low energy using two-loop renormalization-group equations and appropriate threshold effects. The values of A and $\tan\beta$ were determined (as described in Sec. IV above) by fixing the values of (m_b/m_τ) and m_τ. The remaining four parameters of the models—B, C, γ, and ϕ—were used to fit m_c, m_μ, m_e, and $\sin\theta_C$. Predictions were obtained for the eight remaining physical quantities in the quark-lepton mass sector: m_t, m_s, (m_s/m_d), (m_u/m_d), V_{cb}, V_{ub}/V_{cb}, $\tan\beta$, and B_K (or the J). Most of the models are found to fail for one reason or another. For only four choices of 23 operators can the six inputs quantities be self-consistently reproduced as well as giving $V_{cb} = 0.043 \pm 0.007$ and values of m_d/m_s vs m_u/m_d consistent with experiment:

(A) $16_2 45_1 10(1/45_1)16_3 + \gamma e^{i\phi} 16_2 10 45_1 45_{24} 16_3$, (7.5a)

(B) $16_2 45_1 45_1 1016_3 + \gamma e^{i\phi} 16_2 45_{24} 1045_{24} 16_3$, (7.5b)

(C) $16_2 45_1 45_{24} 1016_3 + \gamma e^{i\phi} 16_2 45_1 10(45_{B-L}/45_{24})16_3$, (7.5c)

(D) $16_2 45_1 45_1 1016_3 + \gamma e^{i\phi} 16_2 45_{24} 10(1/45_1)16_3$. (7.5d)

Of these four models, (D) can reasonably be excluded because it predicts $V_{ub}/V_{cb} \leq 0.035$, considerably smaller than the accepted experimental value. V_{ub}/V_{cb} cannot be increased without increasing V_{cb} above 0.053. The other three are consistent with all available experimental data against which we have compared them.

The models (A), (B), and (C) make seven successful predictions for flavor parameters. We present in Figs. 12, 13, and 14 the predictions for $m_t(m_t)$, $\tan\beta$, m_s(1 GeV), V_{cb}, and V_{ub}/V_{cb} vs $\alpha_3(M_Z)$, and (m_s/m_d) vs (m_u/m_d), for models (A), (B), and (C) respectively. Several observations are in order. First, there is a definite lack of universality in the predictions for m_t and $\tan\beta$ vs $\alpha_3(M_Z)$. Model (A), in particular, shows notably different behavior than (B) and (C), with a wider range of permissible values for both m_t and $\tan\beta$, and consequently for $\alpha_3(M_Z)$. In fact, if future experiments support larger values of $\alpha_3(M_Z)$ (≤ 0.12), then only model (A) would remain viable, with a definite prediction of large values for both m_t and $\tan\beta$.

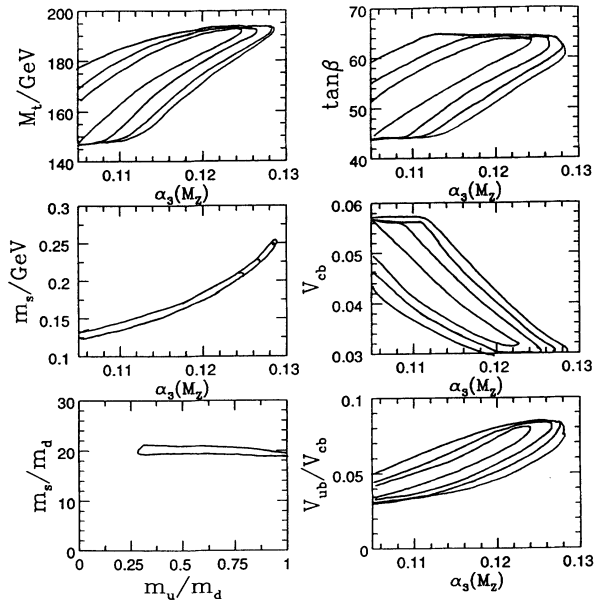

FIG. 12. Predictions for model (A). The variation of the prediction with $\alpha_3(M_Z)$ is shown for the top quark pole mass M_t, $\tan\beta$, m_s(1 GeV), V_{cb}, and V_{ub}/V_{cb}. The prediction for m_s/m_d vs m_u/m_d is also shown. Superpartners are taken degenerate at 200 GeV. The lines are for contours of 0.5σ, 1.0σ, 1.5σ, and 2.0σ for input ranges of $m_b(m_b)=4.25\pm0.25$, $m_c(m_c)=1.27\pm0.05$, and $\sin\theta_C=0.2205\pm0.0018$. Thus, within the innermost contour all three inputs $m_b(m_b)$, $m_c(m_c)$, and $\sin\theta_C$ are within 0.5σ of their central values. In some regions the 1.5σ and 2σ contours are indistinguishable.

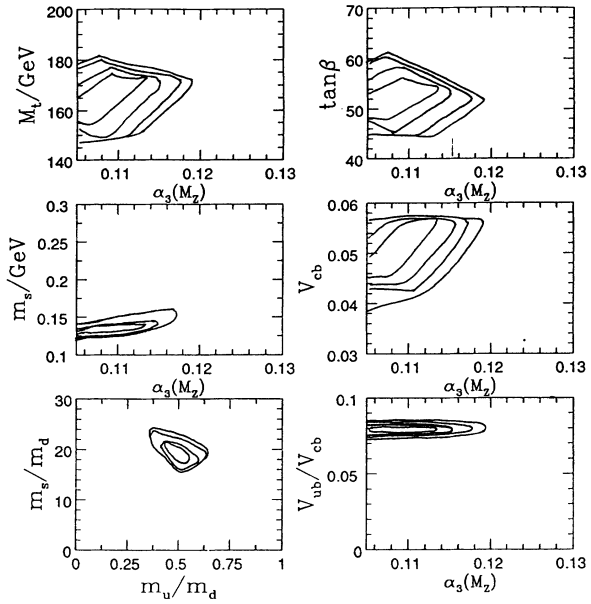

FIG. 13. Predictions for model (B) (same as Fig. 12).

In all three "23" models the top quark can be lighter than in the "22" models. This is due to the modification of the third generation Yukawa coupling eigenvalues by the 23 entries in the Yukawa matrices. In the "22" models these 23 Yukawa entries are typically small, because they are generating the small quantities V_{cb}^2 and λ_c/λ_t. Hence, the correction which they provide to the third generation Yukawa eigenvalues is small (with the notable exception of model 9 where x_e is anomalously large). In the "23" models the situation is considerably different:

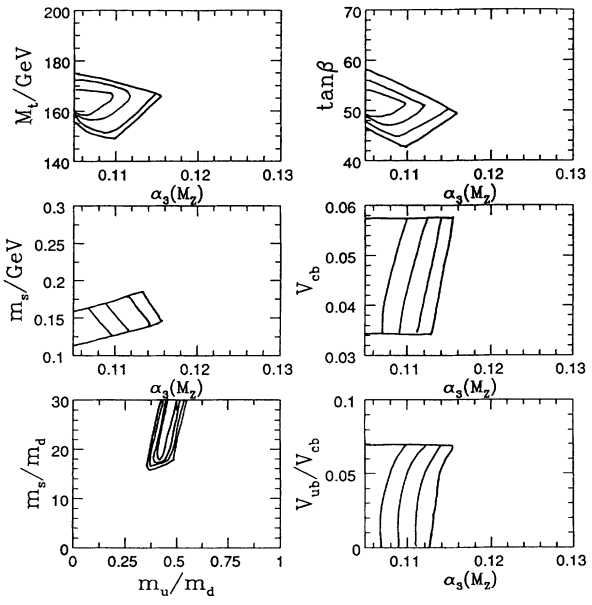

FIG. 14. Predictions for model (C) (same as Fig. 12).

the 23 Yukawa entries must be much larger so that they can account for the larger quantities λ_μ/λ_τ and λ_s/λ_b. The smallness of V_{cb}^2 and λ_c/λ_t is due to an accidental cancellation, as we have stressed. Thus in the "23" models the larger 23 Yukawa entries give considerable corrections to the third generation Yukawa eigenvalues, allowing top quark masses as low as 145 GeV.

All three of the "23" models give remarkably good agreement with the values of m_s/m_d vs m_u/m_d derived from experiment. These are unlikely to be useful in distinguishing between these models.

Tests of these models will come from more accurate measurements of *CP* violation, V_{cb} and V_{ub}/V_{cb}. The predictions for these quantities are correlated since in any given model they must arise from the same set of inputs, in particular, the same value of $\alpha_3(M_Z)$. Using the experimental value for the kaon *CP* impurity parameter ϵ, we can predict the QCD matrix element $\hat{B}_K$, which is shown in Fig. 15 for each of the three models. All are consistent with the lattice result $\hat{B}_K = 0.72 \pm 0.06$ [22], where the error includes only the uncertainty due to the continuum extrapolation. Other calculational approximations, such as the quenched approximation, lead to additional uncertainties. Notice that the prediction of $\hat{B}_K$ is less precise in the "23" models than in the "22" models. This is presumably a reflection of the fact that the "23" models involve a degree of parameter tuning and have predictions which therefore depend sensitively on the inputs. In Figs. 16, 17, and 18 we show, respectively, the correlation of $\hat{B}_K$ with V_{cb}, of $\hat{B}_K$ with V_{ub}/V_{cb}, and of V_{ub}/V_{cb} with V_{cb}. The very tight relationship between $\hat{B}_K$ and V_{cb}, particularly for models (B) and (C), should allow these models to be tested, though not distinguished from each other. If $\hat{B}_K \lesssim 0.7$, then all three models can be distinguished on the basis of their predictions for V_{ub}/V_{cb}. Model (B) can be distinguished in any case by its prediction of $V_{ub}/V_{cb} \simeq 0.08$, the others giving $V_{ub}/V_{cb} \lesssim 0.07$ for $\hat{B}_K \leq 1.5$.

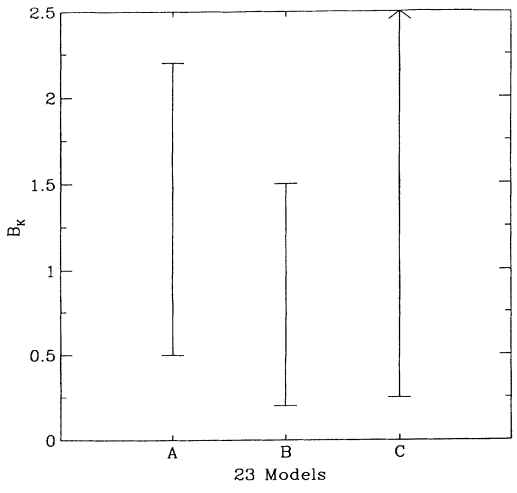

FIG. 15. Prediction for B_K in models (A), (B), and (C). The range corresponds to 2σ variations of the inputs (see Fig. 12), and does not differ greatly from the 1σ allowed regions. The superpartners are taken degenerate with mass 200 GeV.

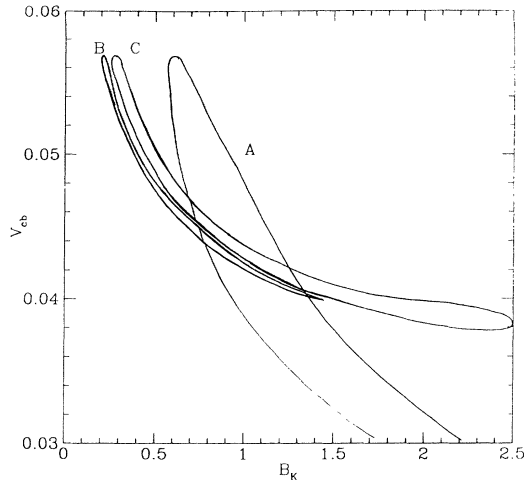

FIG. 16. V_{cb} vs B_K in models (A), (B), and (C). The range corresponds to 2σ variations of the inputs (see Fig. 12), and does not differ greatly from the 1σ allowed regions. The superpartners are taken degenerate with mass 200 GeV.

In Fig. 19 we plot $B_{B_d} F_B^2/\text{GeV}^2$, which for fixed x_d is a measure of $B_d^0 \bar{B}_d^0$ mixing [cf. Eq. (5.44)]. F_B is normalized such that $F_K = 165$ MeV. The most important consequence is that for large values of $\alpha_3(M_Z)$, model (A) favors larger values of $B_{Bd} F_B^2/\text{GeV}^2$.

Finally, we consider *CP* violation in the decays of neutral *B* mesons. Figure 20 shows the predictions for $\sin 2\alpha$ vs $\sin 2\beta$. Here, models (B) and (C) can be separated from each other, since model (B) predicts larger values of $\sin 2\beta$ than model (C). This is largely a reflection of model (B) having larger V_{ub}/V_{cb}. In fact, much of the model (C) region with very low $\sin 2\beta$ is excluded because V_{ub}/V_{cb} is too small. As a demonstration that successful predictions can be obtained simultaneously we provide an example of a particular set of predictions. (See Table VI.)

In this section we have taken all superpartners degen-

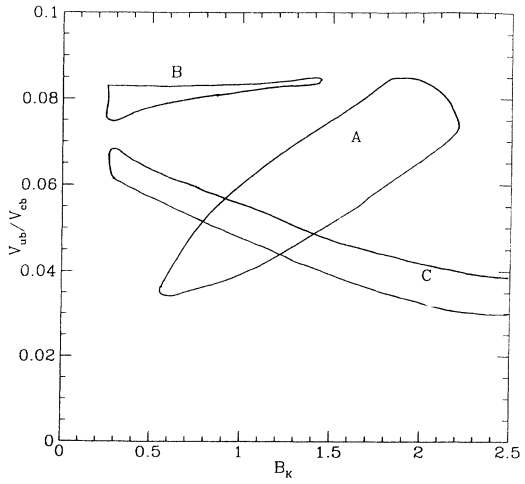

FIG. 17. V_{ub}/V_{cb} vs B_K in models (A), (B), and (C). The range corresponds to 2σ variations of the inputs (see Fig. 12), and does not differ greatly from the 1σ allowed regions. The superpartners are taken degenerate with mass 200 GeV.

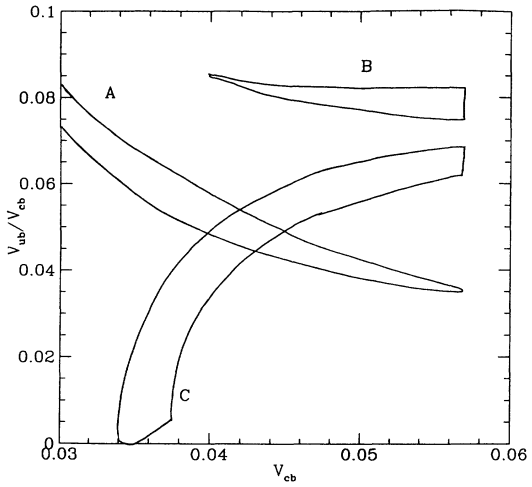

FIG. 18. V_{ub}/V_{cb} vs V_{cb} in models (A), (B), and (C). The range corresponds to 2σ variations of the inputs (see Fig. 12), and does not differ greatly from the 1σ allowed regions. The superpartners are taken degenerate with mass 200 GeV.

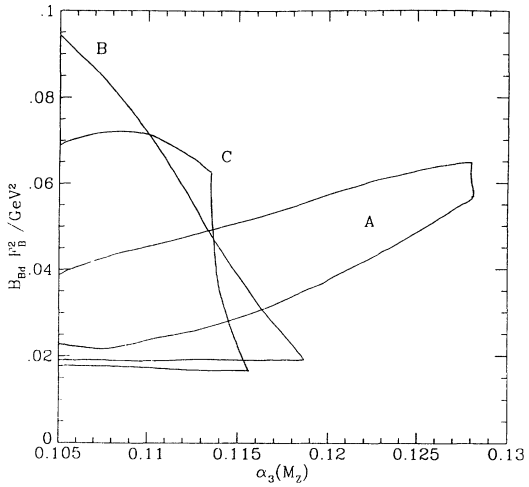

FIG. 19. $B_{B_d}F_B^2$ vs $\alpha_3(M_Z)$ for models (A), (B), and (C). The range corresponds to 2σ variations of the inputs (see Fig. 12), and does not differ greatly from the 1σ allowed regions. The superpartners are taken degenerate with mass 200 GeV.

TABLE VI. Examples of predictions for models (A), (B), and (C).

	Model (A)	Model (B)	Model (C)
$\alpha_1(M_{\rm GUT})$	0.0411	0.0412	0.0412
$\alpha_2(M_{\rm GUT})$	0.0411	0.0412	0.0412
$\alpha_3(M_{\rm GUT})$	0.0400	0.0396	0.0397
$M_{\rm GUT}$/GeV	1.65×10^{16}	1.65×10^{16}	1.65×10^{16}
$M_{\rm SUSY}$/GeV	200	200	200
$\alpha_3(M_Z)$	0.110	0.106	0.107
$\sin^2\theta_W$	0.2325	0.2325	0.2325
A	0.80	0.55	0.575
B/A	0.026 55	0.045 44	0.042 02
C/A	1.223×10^{-4}	1.485×10^{-4}	1.865×10^{-4}
γ	0.931	0.139	0.734
ϕ	3.946	−1.782	0.5125
M_t/GeV	173	159	162
$m_b(m_b)$/GeV	4.16	4.26	4.32
$m_\tau(m_\tau)$/GeV	1.7841	1.7841	1.7841
$\tan\beta$	55.16	50.01	49.75
$m_c(m_c)$/GeV	1.29	1.29	1.27
m_s/MeV	140	137	141
m_μ/MeV	105.658	105.658	105.658
V_{cb}	0.044	0.046	0.044
m_s/m_d	19.7	21.8	22.9
m_u/m_d	0.511	0.451	0.441
m_e/MeV	0.511	0.511	0.511
V_{ub}/V_{cb}	0.046	0.081	0.054
V_{us}	0.2210	0.2202	0.2214
B_K	0.92	0.65	0.86
$\sin2\alpha$	0.32	0.98	0.48
$\sin2\beta$	0.39	0.53	0.45
$\sin2\gamma$	0.08	−0.74	−0.03
$B_{B_d}F_B^2$/GeV²	0.033	0.045	0.037

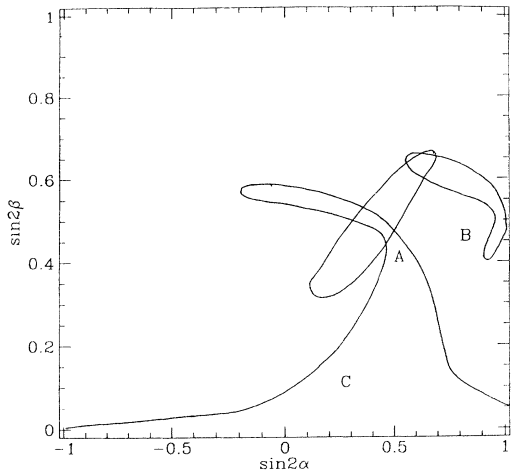

FIG. 20. $\sin 2\beta$ vs $\sin 2\alpha$ for models (A), (B), and (C). The range corresponds to 2σ variations of the inputs (see Fig. 12), and does not differ greatly from the 1σ allowed regions. The superpartners are taken degenerate with mass 200 GeV.

erate at 200 GeV. These predictions of third generation mixing and of *CP* violation are not greatly modified by threshold effects at the weak and/or SUSY scales.

In conclusion, three models of the 23 texture reproduce all the observed masses and mixings of the quarks and leptons. The models give remarkably good agreement for the values of (m_s/m_d) vs (m_u/m_d). They are best tested by the combination of the predictions for V_{cb}, V_{ub}/V_{cb}, and $\hat{B}_K$, and of $\sin 2\beta$ vs $\sin 2\alpha$.

VIII. CONCLUSIONS

In this paper we have explored the consequences of an effective SO(10) grand unified theory with family symmetries which yield very simple and economical flavor structures predicting 7 of the 13 flavor parameters of the standard model. In Sec. III we gave an explicit list of eight assumptions which the theory must satisfy in order that this maximal number of flavor predictions result. Some of these assumptions we believe to be mild and well motivated: they yield the simplest picture in which the weak mixing angle is a significant prediction. Other assumptions are stronger and could easily be violated: for example, it may be that the pattern of family symmetries allows further important flavor operators, or the two Higgs doublets may not lie completely in a single ten-dimensional representation. As each assumption is relaxed the whole picture is not destroyed, rather additional free parameters must be added which successively reduce the predictivity of the theory. We have no compelling reason for why nature should choose the most predictive case; nevertheless, it is appealing to suppose that nature is simple and we find it quite striking that such a predictive possibility is allowed by experiment. We are excited by the prospect that a combination of experiments, each designed to make accurate measurements of parameters of the standard model, could reveal a very simple group theoretic structure underlying the masses and mixings of the quarks and leptons.

In this paper we have discovered and elucidated the predictions of two classes of SO(10) theories which have seven flavor predictions. Every model we have constructed has just a single renormalizable Yukawa coupling which is responsible for m_t, m_b, and m_τ [13,14] and, in most models, this results in a heavy top quark: $M_t = 180 \pm 15$ GeV. We find this picture of third generation Yukawa coupling unification to be rather elegant; however, in Appendix D we warn the reader that it is quite possible to retain the elegance while losing the top mass prediction.

Each of our models has three further operators in the flavor sector, and the models fall into two classes according to whether the resulting texture is of the "22" or "23" type [shown in Eqs. (3.1) and (3.2)]. These additional operators are nonrenormalizable, and have dimension and flavor structure allowing the observed hierarchy of quark and lepton masses and mixings to emerge as a consequence of the small ratio of the grand to Planck mass scales M_G/M_P. The flavor structure of the operators is dictated in a very straightforward way from the observed pattern of nearest-neighbor mixing of the CKM matrix: there must be at least one operator which mixes the heaviest two generations O_{23} and at least one which mixes the lightest two O_{12}. Furthermore, in Appendix B we prove that the fourth operator must be O_{22} or O'_{23}, leading to the two different textures. A very general argument in Appendix A shows that the operator O_{12} is unique, and therefore common to both textures. For models with the "22" texture the operator O_{22} must also lead to unique Yukawa coupling relations. Hence the multiplicity of models which we have discovered, nine for the "22" texture and three for the "23" texture, is a reflection of the many differing operators for the 23 entry.

How significant is the finding of this paper: that the wealth of experimental data on the masses, mixings, and *CP* violation of the quarks and leptons can be described in terms of just four SO(10) invariant operators? The operator search apparently ranges over a vast number of possible operators. If models can typically be found for any values of the masses and mixings then our result is not particularly surprising or significant. This is not the case; the argument is as follows. Models with the minimal number of flavor operators must be of the "22" or "23" texture. The number of possible operators for O_{33}, O_{23}, O_{22}, and O_{12} are 2, 152, 108, and $\approx 3\times 10^4$, respectively. Only one of the O_{33} operators can accommodate the observed value for m_b/m_τ, certainly it would not be possible to accommodate any value. Of the $\approx 3\times 10^4$ possible O_{12} operators, only one is consistent with 60 MeV $< m_s < 360$ MeV, $0.2 < m_u/m_d < 1.5$ and the observed Cabibbo angle. If m_u/m_d had been, for example, 3, our whole program would have collapsed. The uniqueness of O_{12} we believe to be one of our most interesting results. Next consider the operator O_{22} of the "22" texture. It generates the "large" parameters m_s/m_b and m_μ/m_τ, but is not responsible for the "small" parameters m_c/m_t and V_{cb}^2, and hence must give the Clebsch ratios close to the uniquely successful ones of Eq. (5.5): $y_u : y_d : y_e = 0:1:3$. Suppose that the experimental

value of the muon mass had turned out to be twice the usual number, then we would be seeking Clebsch ratios close to $y_u:y_d:y_e=0:1:6$. There are no operators which give Clebsch factors close to this. If the muon mass were doubled (or trebled) our program would fail. The success and uniqueness of the operators O_{33}, O_{22}, and O_{12} is significant and by no means guaranteed. The situation with the operator O_{23} is somewhat different. It is not unique: there are nine possible 23 operators in the "22" textures and three such possible pairs in the "23" texture. This operator generates V_{cb}. If V_{cb} were doubled we could still find acceptable O_{23} operators for the "22" texture. However, if V_{cb} were halved there would be no acceptable operator and our program would again fail. The value of V_{cb} obtained in models 1–4 is the lowest which we can obtain, and these models tend not to have sufficient *CP* violation. A more accurate experimental value of V_{cb} is of very great interest: a reduced error bar will tell us which, if any, O_{23} operator is correct. A low experimental value for V_{cb} would be sufficient to exclude models 5–9, which give a range $0.045<V_{cb}<0.055$.

While models of both textures can be found which agree well with data, we have a theoretical bias towards the models with "22" texture, as those with the "23" texture involve a modest fine-tuning, between the coefficients of O_{23} and O'_{23}, in order to understand the smallness of V_{cb}. The predictions for the models with "22" texture are given with approximate analytic equations in Sec. V and from a numerical calculation in Figs. 1–11. All possible models have been found which satisfy the search criteria of Sec. III A. Of the nine "22" models, four (models 1–4) have difficulty in yielding sufficient *CP* violation in the neutral K system. The remaining 5 models give $0.045<V_{cb}<0.055$. The predictions for the three models with "23" texture are discussed in Sec. VII and numerical results are shown in Figs. 12–20.

It will not be an easy experimental task to distinguish between the models. Nevertheless, we believe that a real test of these models is possible. Each model has seven flavor predictions, with theoretical uncertainties of about 10%. Some theoretical uncertainties at this level are expected from physics at the grand unification scale and hence, without a more detailed theory, probably cannot be removed. It is therefore crucial that these models be tested by the combination of all the predictions. The first stage will involve testing whether any model successfully accommodates improved data on M_t, V_{cb}, and V_{ub}/V_{cb} with an improved value of the strong coupling, which must also be consistent with the m_s/m_d vs m_u/m_d plot. The second stage will be to test the predictions of the models for the *CP*-violating angles $\sin2\alpha$, $\sin2\beta$, and $\sin2\gamma$ in neutral B meson decay, and to test the predictions for $B^0\bar{B}^0$ mixing, for both B_d and B_s.

We have not considered neutrino masses in this paper. Dirac neutrino mass matrices, which mix the left-handed electroweak doublet neutrinos with the right-handed singlet neutrinos, are already fixed by our analysis. However, in order to obtain Majorana masses for the right-handed neutrinos (necessary for a see-saw mechanism) additional operators must be considered.

The predictions of this paper are the consequence of two types of symmetries. The SO(10) grand unified symmetry allows us to view quarks and leptons of a given family as different aspects of a single object, and hence relates the ij entries of the Yukawa coupling matrices **U**, **D**, and **E**. Unfortunately, this elegant grand unified symmetry is not sufficient to yield the predictions. In addition, most of the SO(10) operators which could contribute to these Yukawa couplings should be absent. This can be accomplished by using family symmetries, in the theory defined at M_P, as shown by a specific example in Appendix A. Indeed, if family symmetries are present one *expects* the majority of such operators to typically be absent. For example, consider a U(1) symmetry under which the heaviest generation and the Higgs doublets are neutral, but the lighter two generations have any positive charges. The only allowed renormalizable Yukawa interaction is that for the heaviest generation. All other masses and mixings must be small effects induced by higher dimension operators. The challenge is to understand why the family symmetries should be those which are needed to yield the pattern of non-renormalizable operators which we have found to be singled out by experiment.

ACKNOWLEDGMENTS

G.W.A. thanks Uri Sarid for confirming some numerical data and the Aspen Center for Physics. L.J.H. thanks Riccardo Rattazzi, Graham Ross, and Uri Sarid for many valuable conversations. L.J.H. and S.R. thank Riccardo Barbieri for many illuminating thoughts on the material of Appendix A. G.D.S. thanks ITP at Santa Barbara and the Aspen Center for Physics where part of this work was done. This work was supported by the Director, Office of Energy Research, Office of High Energy and Nuclear Physics, Division of High Energy Physics of the U.S. Department of Energy under Contracts No. DE-AC03-76SF00098 and No. DE-ER-01545-585, and by NSF Grants No. PHY-92-19345 and No. PHY-90-21139.

APPENDIX A

SO(10) grand unification provides a very powerful reduction in the number of free Yukawa parameters: the elements of **D** and **E** can be fixed in terms of those of **U**. However, this parameter reduction by itself is not sufficient to yield predictions: **U** is, in general, a complex 3×3 matrix with 18 parameters. Underlying the search in this paper, for the SO(10) flavor sector with the minimal number of operators, is the belief that such a simple picture will emerge from a set of family symmetries. There must be some set of symmetries which distinguishes between the three families and which explains why the majority of both the renormalizable and nonrenormalizable superpotential interactions are absent at the GUT scale.

This is very straightforward at the renormalizable level. A U(1) symmetry with zero charges for the $\mathbf{16}_3$ and **10**, and positive charges for the $\mathbf{16}_1$ and $\mathbf{16}_2$, immediately leads to a single renormalizable Yukawa interaction: $\mathbf{16}_3$ **10** $\mathbf{16}_3$. This illustrates that it is not difficult to arrange for most couplings to vanish, giving sparse matrices of

couplings. In this appendix we extend this idea to the nonrenormalizable level and given an explicit realization of family symmetries which leads to one of our models. This involves going beyond the effective GUT theory and looking at how the renormalizable operators are obtained by integrating out heavy states at the scale v_{10} or M_P. In addition to providing an understanding of the origin of the flavor structure, this analysis shows that there are corrections to these effective operators, and we estimate the size of such corrections.

In Fig. 21, we show the tree diagrams which lead to one of the "22" texture models (model 9) with $\chi=\frac{8}{9}$ discussed in Sec. IV. The intermediate fermions obtain large masses [of order v_{10} in (B) and (C), and even higher in (D)] and mix with the light states by Higgs VEV's of order M_G. We also display the possible global U(1) family quantum number (in the upper right) which prohibits additional terms in the mass matrix. These diagrams are to be understood as a perturbative technique for integrating out heavy fields and obtaining an approximate mass matrix for the light states. A more detailed analysis of such theories will be given in a future paper, which will provide a complete theory including the SO(10) gauge symmetry breaking sector [12].

To leading order in the small ratios M_G/v_{10} or v_{10}/M_P, the mass matrices for the light fermions are given in terms of the four operators:

$$
\begin{aligned}
O_{33} &= \mathbf{16}_3\ \mathbf{10}\ \mathbf{16}_3\ , \\
O_{23} &= \mathbf{16}_2\mathbf{10}\frac{45^2_{B-L}}{45^2_1}\mathbf{16}_3\ , \\
O_{22} &= \mathbf{16}_2\mathbf{10}\frac{45_{B-L}}{45^2_1}\mathbf{16}_2\ , \\
O_{12} &= \mathbf{16}_1\left[\frac{45_1}{M}\right]^3\mathbf{10}\left[\frac{45_1}{M}\right]^3\mathbf{16}_2\ ,
\end{aligned}
\tag{A1}
$$

where S is an SO(10) singlet fields with VEV's of order M_G. Note that it is necessary to introduce the U(1) in the fundamental theory at M_P since it is only at this level that the ordering of operators can be constrained. For example, it is only at the renormalizable level that symmetries can guarantee that O_{23} in Eq. (A1) will be generated without also giving a similar operator with the **10** appearing next to the $\mathbf{16}_3$.

Having displayed the flavor symmetry structure which leads to the desired operators we now discuss corrections to the mass matrices. The first type of corrections comes from other operators generated via diagrams similar to those in Fig. 21: for example, the operator $O_{13}=\mathbf{16}_1 45_1^3 \mathbf{10}\ 45_1\mathbf{16}_3$. Whether this operator makes an

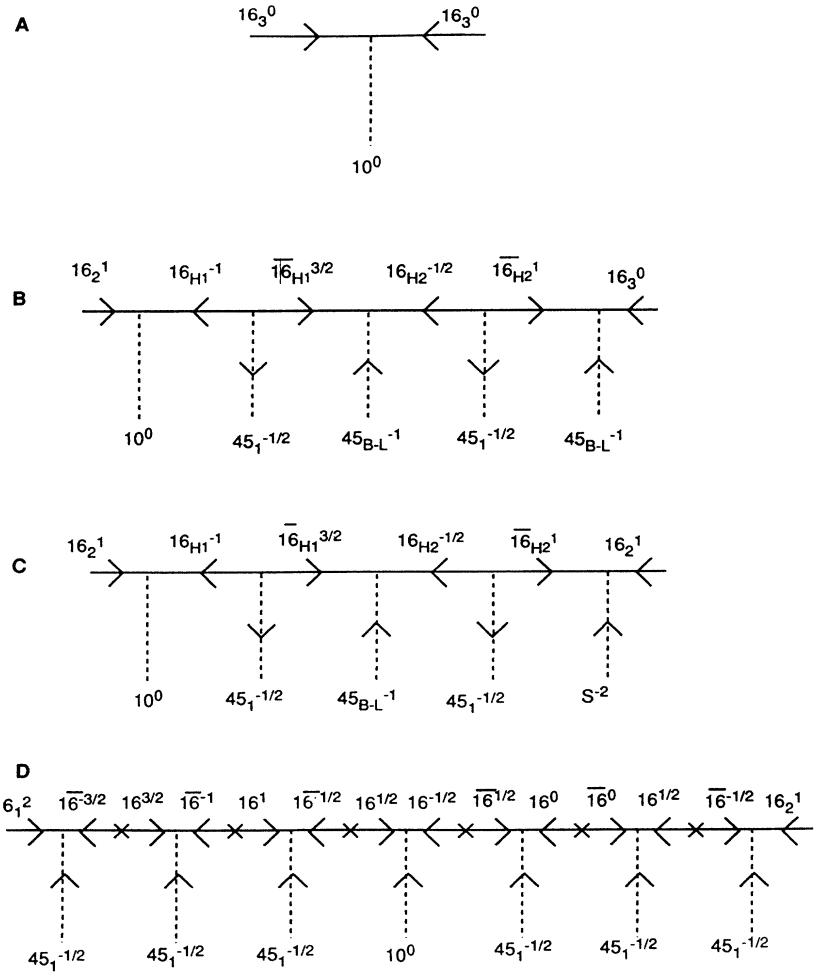

FIG. 21. Diagrams generating the operators of model 9: (a) the Yukawa coupling for the third generation; (b) generation of O_{23} via exchange of superheavy generations; (c) generation of O_{22} via exchange of superheavy generations; (d) generation of O_{12} via exchange of superheavy generations. The superscripts label the charges of the representations under a new U(1) symmetry.

important contribution depends on the relative size of the ratios v_{10}/M_P and v_5/v_{10}. Another operator which is generated from integrating out the superheavy $\overline{16}_{H_2}$ is the $(16_2^\dagger S^\dagger 45_{B-L} 16_3)_D$. At first sight the wave-function mixing generated by this operator is dangerous. However, the new terms induced are actually higher order, as shown by the exact diagonalization performed below. Clearly, the family symmetries may give fermion mass matrices which are dominated by just four operators, but corrections from other operators are generically expected.

A second type of correction to the light fermion mass matrices arises even in the limit that all operators beyond the four dominant ones are neglected. We are considering theories with both superheavy and light 16's. The diagrams of the form of those in Fig. 21 represent an approximation to the process of diagonalizing the mass matrices. We illustrate this in the above example by performing an exact diagonalization of the mass matrices of the heavier two families. In this sector (including all the relevant heavy states) there are two $\overline{16}$'s and four 16's which we denote as

$$\bar{f}_i = \overline{16}_{H_i}, \quad i=1,2 , \tag{A2}$$

f_a, $a=1,\ldots,4$ where

$$f_1 = 16_{H_1}, \quad f_2 = 16_{H_2}, \quad f_3 = 16_2, \quad f_4 = 16_3 , \tag{A3}$$

and f_3 and f_4 are to leading order the light second and third families, respectively. The fundamental mass term in the Lagrangian is given by

$$\bar{f}_i m_{ia} f_a \tag{A4}$$

with the 2×4 mass matrix

$$m_{ia} = \begin{bmatrix} 45_1 & 45_{B-L} & 0 & 0 \\ 0 & 45_1 & S & 45_{B-L} \end{bmatrix} . \tag{A5}$$

The quadratic mass matrix $m^2 \equiv \sum_{i=1}^2 m_{ia} m_{ib}^*$ is Hermitian and can be diagonalized by a unitary transformation. In this case we have

$$m^2 = \begin{bmatrix} 45_1^2 & 45_1 45_{B-L} & 0 & 0 \\ 45_1 45_{B-L} & 45_1^2 + 45_{B-L}^2 & 45_1 S & 45_1 45_{B-L} \\ 0 & 45_1 S & S^2 & S 45_{B-L} \\ 0 & 45_1 45_{B-L} & S 45_{B-L} & 45_{B-L}^2 \end{bmatrix} , \tag{A6}$$

where for simplicity the VEV's are taken to be real. The eigenstates are given by

$$f'_a = V_{ab} f_b \quad \text{and} \quad f_a = V_{ba}^* f'_b . \tag{A7}$$

If we denote the massless eigenstates by f'_3 and f'_4, we find the exact solutions

$$f_4 = V_{44}^* f'_4 + V_{34}^* f'_3 + \cdots , \tag{A8a}$$

$$f_3 = V_{43}^* f'_4 + V_{33}^* f'_3 + \cdots , \tag{A8b}$$

$$f_1 = V_{41}^* f'_4 + V_{31}^* f'_3 + \cdots \tag{A8c}$$

with the ellipsis representing the contribution of the massive modes and

$$V_{44} = \frac{1}{\sqrt{1+\alpha_1^2+\alpha_2^2+\alpha_3^2}}, \quad V_{34} = 0 ,$$

$$V_{43} = \frac{\alpha_3}{\sqrt{1+\alpha_1^2+\alpha_2^2+\alpha_3^2}}, \quad V_{33} = \frac{1}{\sqrt{1+\beta_1^2+\beta_2^2}} ,$$

$$V_{41} = \frac{\alpha_1}{\sqrt{1+\alpha_1^2+\alpha_2^2+\alpha_3^2}}, \quad V_{31} = \frac{\beta_1}{\sqrt{1+\beta_1^2+\beta_2^2}} ,$$

where

$$\beta_1 = \frac{45_{B-L} S}{45_1^2}, \quad \beta_2 = -\frac{S}{45_1} ,$$

$$\alpha_1 = -\frac{45_{B-L}}{45_1}\alpha_2 ,$$

$$\alpha_2 = -\frac{45_{B-L}}{45_1}\left[1+\frac{S^2}{45_1^2}+\left[\frac{45_{B-L} S}{45_1^2}\right]^2\right]^{-1} ,$$

$$\alpha_3 = -(\beta_1\alpha_1+\beta_2\alpha_2) .$$

We can now evaluate the electroweak symmetry-breaking mass terms due to the Higgs scalars sitting in the ten-dimensional representation. We have

$$16_3 10\ 16_3 + 16_2 10\ 16_{H_1} = f_4 10 f_4 + f_3 10 f_1 . \tag{A9}$$

We now use Eq. (A8) to rewrite (A9) in terms of the massless fields f'_4 and f'_3. This gives us our effective operators O_{ij}. We also relabel the states $f'_4 \to 16_3$ and $f'_3 \to 16_2$ in order to obtain formulas similar to that of Eq. (A1). We have

$$O_{33} = 16_3 (V_{44}^* 10 V_{44}^* + V_{43}^* 10 V_{41}^*) 16_3 , \tag{A10a}$$

$$O_{23} = 16_2 (V_{31}^* 10 V_{43}^* + V_{33}^* 10 V_{41}^*) 16_3 , \tag{A10b}$$

$$O_{22} = 16_2 V_{33}^* 10 V_{31}^* 16_2 . \tag{A10c}$$

To leading order we obtain the operators, O_{33} [Eq. (2.1)], O_{22} [Eq. (5.6f)], and O_{23}, the third operator with $\chi = \frac{8}{9}$ in Eq. (5.12c). The relative corrections to the leading-order results are of order $45_{B-L}^2/45_1^2$ or $S^2/45_1^2$ which may be as large as 10%. It should also be noted that these corrections include Clebsch factors which differ for up and down quarks and leptons. Finally, it is instructive to notice that if the "22" element vanishes in the up mass matrix to leading order then this result is true for the exact mass matrix as obtained above [Eq. (A10c)].

APPENDIX B

In this appendix we use experimental data to exclude theories with the heavy 2×2 sector given only in terms of two operators, $O_{33}+O_{23}$, where O_{33} is given in (2.1) and O_{23} has the form of (2.2) and has dimension ≤ 6. The operator O_{33} works very well for the heaviest generation. The difficulty arises in finding a suitable O_{23} to account for the four observables V_{cb}^2, m_c/m_t, m_s/m_b, and m_μ/m_τ. This is largely because the first two of these

quantities are considerably smaller than the second two, as shown in (5.4e).

The Yukawa matrices of the two heavy families 16_3 and 16_2 at the GUT scale are given by

$$\mathbf{U}=\begin{bmatrix} 0 & x_u' B \\ x_u B & A \end{bmatrix}, \quad \mathbf{D}=\begin{bmatrix} 0 & x_d' B \\ x_d B & A \end{bmatrix}, \quad \mathbf{E}=\begin{bmatrix} 0 & x_e' B \\ x_e B & A \end{bmatrix}, \tag{B1}$$

where the x_i and x_i' are the Clebsch factors resulting from the operator O_{23}. The two operator coefficients, A and B, have been made real by phase rotations on 16_2 and 16_3. From these Yukawa matrices it follows that, at M_G,

$$\frac{\lambda_t}{\lambda_c}x_u x_u' = \frac{\lambda_b}{\lambda_s}x_d x_d' = \frac{\lambda_\tau}{\lambda_\mu}x_e x_e' = \frac{|x_u - x_d|^2}{V_{cb}^2} \equiv \frac{A^2}{B^2} \tag{B2}$$

giving the GUT relations

$$\xi \equiv \frac{x_d x_d'}{x_u x_u'} = \frac{\lambda_t}{\lambda_b}\frac{\lambda_s}{\lambda_c}, \tag{B3}$$

$$\chi \equiv \frac{|x_u - x_d|}{\sqrt{|x_u x_u'|}} = V_{cb}\left[\frac{\lambda_t}{\lambda_c}\right]^{1/2}. \tag{B4}$$

Using the analysis of Sec. IV to scale the quantities on the right-hand sides to low energies gives

$$\xi = \frac{m_t}{m_c}\frac{m_s}{m_b}\frac{\eta_b \eta_c}{\eta_s}e^{2(I_t - I_b)}, \tag{B5}$$

$$\chi = V_{cb}\left[\frac{m_t}{m_c}\right]^{1/2}\sqrt{\eta_c}\,e^{(I_t - I_b)/2}. \tag{B6}$$

Using experimental values for m_c, m_b, and V_{cb}, together with the prediction for $m_t(\alpha_s)$ which follows from O_{33} and the values of the scaling factors $\eta_i(\alpha_s)$, $I_t(\alpha_s)$, and $I_b(\alpha_s)$ we find the numerical values

$$0.55 < \chi < 0.92, \qquad 4\frac{m_s}{100\ \text{MeV}} < \xi < 7\frac{m_s}{100\ \text{MeV}}, \tag{B7}$$

where variation is due to $0.11 < \alpha_s < 0.13$. For the purposes of this appendix we will discard models only if they are in gross disagreement with (B7); in particular, if they are outside the range

$$0 < \chi < 2, \qquad 1 < \xi < \infty. \tag{B8}$$

From the table it is immediate to see that the only dimension-5 operators giving $\xi > 1$ are $\mathbf{16}_2(\mathbf{45}_1/M)\mathbf{10}\ \mathbf{16}_3$ or $\mathbf{16}_2\mathbf{10}(\mathbf{45}_1/M)\mathbf{16}_3$: they both give $\xi = 3$. However, the former gives $\chi = 0$ and the latter $\chi = 4$ so they are not acceptable.

Now consider dimension 6 operators. Note that $\mathbf{45}_{T_3R}$ may not appear since it gives $m_c = m_s = m_\mu = 0$. Furthermore, the appearance of $\mathbf{45}_{B-L}$ is irrelevant: it does not distinguish between the up and down sectors and hence will not affect ξ or χ. Hence, we need only consider $\mathbf{45}_1$ and $\mathbf{45}_{24}$. Since $\mathbf{45}_{24}$ leads to $\xi < 1$, there must be more $\mathbf{45}_1$'s appearing in the numerator than in the denominator to ensure $\xi > 1$. At dimension 6 this implies that either one or two $\mathbf{45}_1$'s are in the numerator and none in the denominator, which already implies $\chi \geq 1$. In fact, dimension-6 models constructed from $\mathbf{45}_1$ and $\mathbf{45}_{24}$ all have $\chi = 0$ or $\chi \geq 2$ and hence are excluded.

These arguments show that a correct description of the heavier two families requires the addition of a third operator. The alternatives are (a) add an operator mixing $\mathbf{16}_2$ with $\mathbf{16}_2$ ("22" models), (b) add one more operator mixing $\mathbf{16}_2$ with $\mathbf{16}_3$ ("23" models), or (c) add one more higher dimension operator mixing $\mathbf{16}_3$ with $\mathbf{16}_3$.

It is easy to see that the last option (c) will not help. The higher dimension operator will make a $\leq 20\%$ change in the $\mathbf{16}_3\mathbf{16}_3$ entries of the mass matrices. Such a change will alter the allowed ranges of ξ and χ given in (B7) by $\approx 20\%$. However, we have already proven that no model met the very much weaker constraints of (B8), and hence (c) will not yield an acceptable model.

This concludes the proof that we need to consider theories of type (a) or (b).

What about anti-SU(5) theories? As we shall see later they are excluded by considering the "12" entry of the mass matrices.

APPENDIX C

In this appendix we show that for the theories introduced in Sec. III, which have fermion masses described by four SO(10) operators, the operator which gives rise to the 12 element of the mass matrices is unique. This relies only on the 33 operator being $\mathbf{16}_3\ \mathbf{10}\ \mathbf{16}_3$, and does not depend on the form of the 22 or 23 operators. In fact it applies to both the "22" and "23" textures.

From the determinant of the light 2×2 sector of the mass matrices one derives

$$\frac{m_d m_s}{m_e m_\mu} = \left[\frac{m_b}{m_\tau}\right]^2 \frac{z_d z_d'}{z_e z_e'}\frac{\eta_d \eta_s}{\eta_b^2}\frac{\eta_\tau^2}{\eta_e \eta_\mu}e^{2I_t + 6I_b - 6I_\tau}. \tag{C1}$$

Inputting m_e, m_μ, m_τ, m_b, and $m_s/m_d = 20$ leads to a result for the strange mass:

$$m_s \simeq 180\ \text{MeV}\left[\frac{z_d z_d'}{z_e z_e'}\right]^{1/2}\frac{\sqrt{\eta_d \eta_s}}{\eta_b}\frac{e^{I_t + 3I_b - 3I_\tau}}{2.3}. \tag{C2}$$

Thus a strange mass of 180 MeV results only if $z_d z_d'/z_e z_e'$ is close to unity [in fact, 1 to 1.7 as $\alpha_s(M_Z)$ decreases from 0.13 to 0.11]. This is not a surprising result. Once $(\lambda_\mu/\lambda_s)_G = 3$ has been arranged, we know from Georgi and Jarlskog's work that the 12 entries should be the same for the down and lepton matrices. Given that several 45 VEV's are expected to occur in the 12 operator, how can we arrange for $z_d z_d' = z_e z_e'$? One possibility is that the 12 operator involves only $\mathbf{45}_1$. In this case the Clebsch factors z_i and z_i' do not feel SU(5) breaking in the e and d sectors so that $z_d z_d' = z_e z_e'$ is automatic. At first thought, one might guess that there would be other ways

to arrange a product of many 45's (involving 45_{B-L} 45_{T_3R} and 45_{24} as well as 45_1) such that $z_d z_d' \simeq z_e z_e'$ occurs as an accident. In fact, it is very straightforward to see that this is impossible. From the Clebsch table we see that the appearance of 45_{T_3R} in the 12 operator is forbidden as it leads to $z_i z_i' = 0$. Furthermore, the appearance of either a 45_{24} or a 45_{B-L} leads to a factor of 9 appearing in $z_e z_e'/z_d z_d'$. Since there is no possibility of any nonzero factor less than unity contributing to $z_e z_e'/z_d z_d'$, we can immediately use the result (C2) to conclude that the 12 operator can involve only 45's with VEV's pointing in the SU(5) preserving direction: 45_1, i.e.,

$$O_{12} = 16_1 \left[\frac{45_1}{M}\right]^n 10 \left[\frac{45_1}{M}\right]^m 16_2 , \tag{C3}$$

where n and m are positive or negative integers.

We can also use the strange mass prediction of (C2) to exclude any model where SO(10) is broken to the anti-SU(5) subgroup, so 45_1 lies in an anti-SU(5) singlet direction. In this case the z_i, z_i' must be replaced by the $\bar{z}_i, \bar{z}_i'$ relevant to the anti-SU(5) subgroup. Thus m_s^2 is proportional to the $\bar{z}_d \bar{z}_d'/\bar{z}_e \bar{z}_e' = z_u z_u'/z_\nu z_\nu'$. From the Clebsch table one immediately sees that any 45 VEV gives this ratio very far from unity: either zero or ≥ 9. The remaining possibility, $n = m = 0$, we exclude because it is completely unreasonable that in our framework the masses of the lightest generation would arise from a dimension-4 renormalizable operator.

A stringent restriction on n and m can be obtained by considering the determinant of the light 2×2 submatrices in the up and down sector:

$$\frac{m_u m_c}{m_d m_s} = \left[\frac{m_t}{m_b}\right]^2 \frac{z_u z_u'}{z_d z_d'} \frac{\eta_u \eta_c}{\eta_d \eta_s} \eta_b^2 e^{4(I_t - I_b)} . \tag{C4}$$

From the Clebsch table,

$$\frac{z_u z_u'}{z_d z_d'} = \left[\frac{1}{3}\right]^{n+m} . \tag{C5}$$

Hence we find

$$\frac{m_u}{m_d} \simeq 0.9 \left[\frac{1}{3}\right]^{n+m-6} \left[\frac{m_s}{180\ \text{MeV}}\right] \eta , \tag{C6}$$

where $\eta = (0.6, 1, 1.1)$ for $\alpha_s(M_Z) = (0.11, 0.12, 0.13)$. Thus even allowing the very wide range $0.2 < m_u/m_d < 1.5$, one can conclude that

$$n + m = 6 \text{ or } 7 . \tag{C7}$$

The third and final part of the argument follows from the prediction for the Cabibbo angle. From the KM matrix of Eq. (4.3) one finds $\sin\theta_C = |s_1 + s_2 e^{-i\phi}|$. The 12 and 21 entries of the up mass matrix are symmetric so that

$$s_2 = \left[\frac{\lambda_u}{\lambda_c}\right]^{1/2} = \left[\frac{\eta_c}{\eta_u}\frac{m_u}{m_c}\right]^{1/2} .$$

However, this symmetry is not necessarily true for the down matrix so that

$$s_1 = \left[\left[\frac{1}{3}\right]^{n-m} \frac{m_d}{m_s}\right]^{1/2} .$$

Because s_2 is considerably less than $\sin\theta_C$ one must have s_1 in the neighborhood of $\sin\theta_C$. As $\sqrt{m_d/m_s} = 0.22 \pm 0.02$ is actually centered on $\sin\theta_C$, having $n \neq m$ makes s_1 too different from $\sin\theta_C$ to obtain a successful result. In fact, the only case with $n \neq m$ which comes even close to working is $n = 4$ and $m = 3$. This case is excluded by combining the Cabibbo angle constraint with the result of (C6) which gives $m_u/m_d < 0.4$. Hence, we are left with the case $n = m = 3$ and the unique operator

$$O_{12} = \psi_1 \left[\frac{45_1}{M}\right]^3 10 \left[\frac{45_1}{M}\right]^3 \psi_2 . \tag{C8}$$

APPENDIX D

This appendix examines the supersymmetric threshold corrections to Yukawa couplings. The top mass prediction of Fig. 1 is large: about two standard deviations above the central value extracted from precision electroweak data in the MSSM. If searches for the top quark prove that the top is indeed this heavy, the case for the scheme proposed in this paper will be strengthened, but by no means proved. If the top quark is found to be much lighter, for example, 140 GeV, it is important to know to what extent the framework of this paper is destroyed.

There are several mechanisms which could affect, to varying degrees, our top mass prediction.

Even if none of the assumptions listed in Sec. III are relaxed, there is an effect which can perturb the top prediction. The equality $\lambda_t = \lambda_b = \lambda_\tau$ is exact at the GUT scale in the limit that the higher dimension operators are ignored. However, the operator O_{23} perturbs this relation, as shown in Eq. (6.1). In the "22" models this is negligible (except for model 9), but in the "23" models it is important, as can be seen in the predictions for the top mass in Figs. 12–14. Other mechanisms affecting m_t require that at least one of the assumptions of Sec. III be relaxed.

It could be that GUT-scale threshold effects, such as an additional nonrenormalizable operator, upset the GUT-scale relation $\lambda_t = \lambda_b = \lambda_\tau$. Such perturbations could arise when assumptions 3, 6, or 7 of Sec. III are relaxed, and are considered in Appendix E.

The supersymmetric threshold corrections to λ_b could be significant if the last assumption of Sec. III is relaxed, and it is this possibility that we explore in this appendix.

While the tree-level contribution to the b and τ masses are proportional to the small VEV v_1, there are one-loop diagrams with internal superpartners which are proportional to v_2. Hence for $\tan\beta \approx 50$ the radiative corrections are naively $\approx 50\%$ rather than $\approx 1\%$. Such radiative corrections imply that the quark and lepton mass predictions could depend on the soft supersymmetry-breaking parameters which appear in these loop diagrams. This would make it impossible to give precise nu-

merical predictions until the superpartner sector has been discovered and studied.

As an example, consider a radiative correction to the b quark mass which is 35% of the tree result, and which subtracts from the tree result. This means that the tree b quark Yukawa coupling, which is the input needed for the top mass prediction, is now 35% larger, resulting in a decrease in the top mass predicted from operator (2.1) by about 30 GeV. The leading radiative corrections to the b quark mass are from gluino and Higgsino exchange diagrams [14] shown in Fig. 22. In the gluino exchange diagram there is a trilinear scalar interaction proportional to μ while in the Higgsino exchange diagram it is proportional to A. For small μ the gluino exchange diagram yields

$$\frac{\delta m_b}{m_b}=\frac{2\alpha_s}{3\pi}\tan\beta\frac{\tilde{m}\mu}{m^2}I\left[\frac{\tilde{m}^2}{m^2}\right] \tag{D1}$$

where, in the limit that the two b squarks are nearly degenerate with mass m, and the gluino has mass $\tilde{m}$

$$I(x)=\frac{1+[x/(1-x)]\ln x}{1-x}\ . \tag{D2}$$

We can divide the parameter space of the MSSM into two regions according to whether these one-loop radiative corrections cause substantial changes to the tree-level predictions. If the corrections are substantial then some of the fermion mass predictions will depend on the parameters m, $\tilde{m}$, μ, and A. The region where these corrections can be ignored is, roughly speaking, that where μ, and probably $\tilde{m}$ and A, are less than the squark mass m.

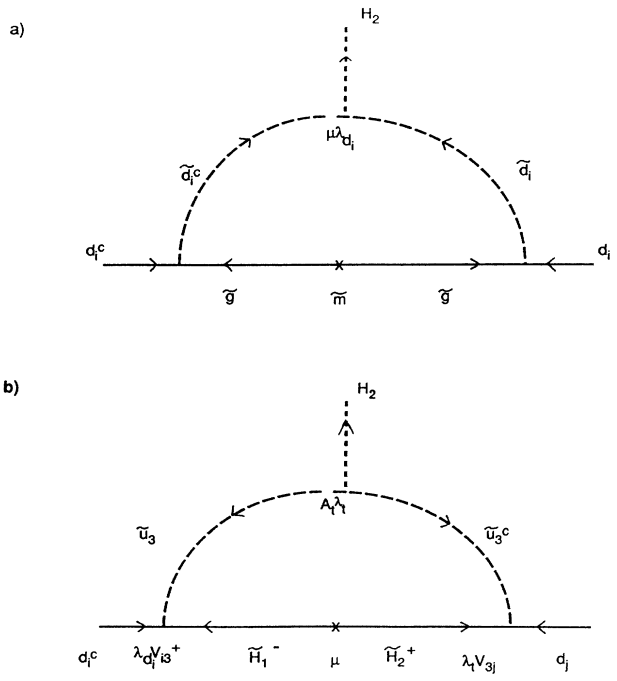

FIG. 22. Supersymmetric threshold corrections to the Yukawa couplings of the down-type quarks from (a) gluino exchange and (b) charged Higgsino exchange. Tildes denote superpartners and V is the CKM matrix.

This region of parameter space is preferred when $\tan\beta$ is large [14]. The Higgs potential of the MSSM involves three parameters: μ_1^2, μ_2^2, and μ_3^2. One combination of these is determined by the constraint of the observed Z mass. The other two parameters can be taken as $\tan\beta$ and the pseudoscalar mass m_A [29]. For large $\tan\beta$ one finds $\mu_3^2=m_A^2/\tan\beta$. Thus large $\tan\beta$ forces $\mu_3^2=\mu B$ to be small, which is most naturally accomplished by a combination of approximate Peccei-Quinn ($\mu/m\approx\epsilon_{\rm PQ}\ll 1$) and R ($\tilde{m}/m\approx A/m\approx B/m\approx\epsilon_R\ll 1$) symmetries. The potentially large radiative corrections to m_b, such as in Eq. (D1), are all proportional to $\epsilon_{\rm PQ}\epsilon_R\tan\beta$ which is expected to be of order unity, because it is the above approximate symmetries which are the origin of small $\cot\beta$: $\cot\beta\approx\epsilon_{\rm PQ}\epsilon_R$. Hence, these radiative corrections are not typically expected to be sufficiently large to substantially alter the predictions of the flavor parameters and are ignored in the body of this paper. Note, however, that we cannot *exclude* the case where they are significant, which would happen, for example, if $\tilde{m}/B\approx 5$. In this case the top quark could be much lighter than our prediction shown in Fig. 1. Nevertheless, the other predictions survive with slight modifications, as discussed later in this Appendix.

Diagrams similar to those which correct the b quark mass (one of the external b quarks becomes an s quark, and a photon is attached) lead to an amplitude for $b\to s\gamma$ linear in $\tan\beta$. Thus the possibility of sizable radiative corrections to m_b can be probed via $b\to s\gamma$ [16].

The suggestion [14] that the small value of m_b/m_t is due to approximate Peccei-Quinn and R symmetries deserves further attention, both from the viewpoint of the radiative mechanism for electroweak symmetry breaking and the resulting experimental signatures (both charginos are expected to have light masses ≈ 100 GeV). What are the origins of these approximate symmetries? An approximate Peccei-Quinn symmetry requires μ to be less than the size of the supersymmetry-breaking parameters. These scales are logically independent; their equality is often called the "μ" problem. In one solution of this problem the μ parameter arises as a radiative correction from the supersymmetry-breaking scale, and is expected to be small [30]. The approximate R symmetry, on the other hand, must result from the particular pattern of supersymmetry breaking.

Now let us consider radiative corrections to our results in more detail. The diagrams of Fig. 22 lead to supersymmetric threshold corrections to $\delta m_b/m_b$, which are naively $\alpha_s/4\pi$ and $\lambda_t^2/16\pi^2$, respectively, which are both $\approx 1\%$. These diagrams yield [14]

$$\frac{\delta m_b}{m_b}\sim\frac{2\alpha_3}{4\pi}\left[\frac{m_{1/2}}{B}\right]\left[\frac{m_A^2}{m_0^2}\right], \tag{D3}$$

$$\frac{\delta m_b}{m_b}\sim\frac{\lambda_t^2}{16\pi^2}\left[\frac{A_t}{B}\right]\left[\frac{m_A^2}{m_0^2}\right], \tag{D4}$$

where A_t, B, and $m_{1/2}$ are supersymmetry-breaking parameters, m_A is the mass of the pseudoscalar of the MSSM, and m_0 characterizes the mass scale of the degen-

erate scalar superpartners. The most natural expectation is that $A_t \sim B \sim m_{1/2}$ and $m_A < m_0$ in which case $\delta m_b/m_b < 2\%$ and 2/3%, respectively, so that the top mass is changed by less than 3 GeV. The most natural expectation is that these radiative corrections do not substantially change the predictions shown in Fig. 1. Nevertheless, it is not extremely unnatural for, for example, $m_{1/2}/B \sim 5$ or 10, which could lower the top mass prediction by 15–30 GeV. The sign of the diagrams is unknown because the sign of μ is unknown, in this section we are interested in the sign which leads to a decrease in m_t.

The effects of δm_b can be understood as follows: the b Yukawa coupling gets multiplied by a factor $(1-\xi)$, so that in Eq. (4.10) $\eta_b \to \eta_b(1-\xi)$. Thus the changes are identical to those that would occur if the physical b mass, m_b, were multiplied by $1/(1-\xi)$. For ξ positive this increases m_b, and the resulting decreases in M_t and $\tan\beta$ can now be read from Figs. 1(a) and 1(b).

The leading effects of this λ_b threshold correction on the other predictions of the "22" models can now be obtained from Eqs. (5.33)–(5.37) by multiplying m_b by $1/(1-\xi) \sim (1+\xi)$ and using the corrected value for m_t. Subleading corrections arise because the Yukawa coupling A has changed, inducing a change in the integrals $I_{t,b,\tau}$.

However, some of these predictions are also affected by threshold corrections to other elements of the down Yukawa matrix which result from Figs. 22(a) and 22(b). In this appendix we consider these corrections in the following approximation. We ignore the RG scaling of the down-type squark mass matrix, and of the down-type A matrix, except for the effect which makes $\tilde{b}$ not degenerate with $\tilde{s}$ and $\tilde{d}$. In this approximation the gluino exchange diagram conserves flavor, so that its only additional effect is to give equal threshold corrections to λ_s and λ_d. This can be accounted for by multiplying the predictions for m_s and m_d by $1-\xi'$, where ξ' has the same sign as ξ and is equal to it in the limit of squark degeneracy. Hence the leading effects of the gluino exchange diagram are (1) m_t multiplied by $(1-0.8\xi)$, (2) $\tan\beta$ multiplied by $(1-1.7\xi)$, (3) V_{cb} multiplied by $(1+0.4\xi)$, (4) m_s multiplied by $(1+\xi)/(1+\xi')$, (5) m_s/m_d unchanged, (6) m_u/m_d multiplied by $(1-2.6\xi)/(1+\xi')$, (7) V_{ub}/V_{cb} multiplied by $(1-0.8\xi)$, and (8) J unchanged.

We see that if the supersymmetric threshold corrections are surprisingly big, for example $\xi = 0.1$–0.2, our top mass prediction is largely lost, but the other predictions are simply perturbed. The most interesting change is for m_u/m_d, since it is decreased and this improves the agreement with experiment in all "22" models.

The Higgsino exchange diagram of Fig. 22(b) is typically smaller than the gluino exchange diagram of Fig. 22(a). The flavor structure of this diagram is more complicated than for the gluino exchange diagram because the charged Higgsino vertices contain a factor of the CKM matrix. Nevertheless, the diagram is extremely small unless the exchanged scalar is from the third generation, and the only operators generated significantly are bb^c, sb^c, and db^c. The first contributes to ξ as above, while the others perturb V_{cb} and V_{ub}.

APPENDIX E

In this appendix we consider the effects of GUT-scale threshold corrections perturbing the boundary conditions on the Yukawa matrices. This could occur in many ways; we will just consider some simple cases for which there may be some motivation.

The Yukawa couplings of the third generation, U_{33}, D_{33}, and E_{33} can be perturbed by the presence of an additional nonrenormalizable operator. This could allow $\lambda_t > \lambda_b$ at the GUT scale, which may be the easiest way to allow radiative electroweak symmetry breaking. If this extra operator gives contributions to the Yukawa couplings which preserve SU(5), for example,

$$O'_{33} = \mathbf{16}_3 \mathbf{10}\ \mathbf{45}_1 \mathbf{16}_3 , \tag{E1}$$

then the t Yukawa can increase slightly, by a correction v_{10}/M_P, compared with the b and τ couplings, which remain equal. Such a perturbation in the boundary conditions leads to a very small change in the top mass prediction [14]: about 2 GeV for $v_{10}/M_P = 0.2$. Other predictions are also affected insignificantly. If $\mathbf{45}_1$ is replaced by 45_Y in Eq. (E1), the b and τ couplings will no longer be equal at the GUT scale. The relation (4.10) for m_b/m_τ will be multiplied by some correction factor, $(1-\xi)$, and this can substantially decrease the top mass and perturb other predictions as described in Appendix D.

Finally, we consider the violation of assumption 3, that both Higgs doublets of the MSSM lie entirely in a single 10. Suppose that all Yukawa interactions are generated by the couplings of a single 10, but this 10 contains only components of the two light Higgs doublets. The other components must come from some other representation 10′, 120, 126, etc. The effect is to multiply the Yukawa matrix **U** by one mixing angle and **D** and **E** by another. The mixing angle which multiplies **U** can be absorbed into the coupling constants, so the net result is to simply multiply **D** and **E** by some number ζ. The effect of ζ is to rescale $\tan\beta$. For example Eq. (4.10) for m_b/m_τ is unchanged, but in Eq. (4.11) $\cos\beta$ must be multiplied by ζ. With ζ very small there is no need for $\tan\beta$ to be large, so electroweak symmetry breaking could occur without any fine tuning. The one extra free parameter, ζ, means that $\tan\beta$ can no longer be predicted. Even though the top Yukawa can be predicted, the top quark mass prediction, which is proportional to $\lambda_t \sin\beta$, is lost. The remaining six flavor predictions for each of the "22" models are given by the same expressions as before. The numerical values for the predictions will change slightly due to the change in the integrals $I_{t,b,\tau}$.

[1] H. Georgi and S. Glashow, Phys. Rev. Lett. **32**, 438 (1974); H. Georgi, H. Quinn, and S. Weinberg, *ibid.* **33**, 451 (1974).

[2] S. Dimopoulos, S. Raby, and F. Wilczek, Phys. Rev. D **24**, 1681 (1981); S. Dimopoulos and H. Georgi, Nucl. Phys. **B193**, 150 (1981); L. Ibanez and G. G. Ross, Phys. Lett. **105B**, 439 (1981); M. B. Einhorn and D. R. T. Jones, Nucl. Phys. **B196**, 475 (1982); W. J. Marciano and G. Senjanovic, Phys. Rev. D **25**, 3092 (1982).

[3] R. Barbieri, CERN Report No. CERN 6863/93 (unpublished).

[4] H. Georgi and C. Jarlskog, Phys. Lett. **86B**, 297 (1979); H. Georgi and D. V. Nanopoulos, Nucl. Phys. **B159**, 16 (1979); J. Harvey, P. Ramond, and D. B. Reiss, Phys. Lett. **92B**, 309 (1980); Nucl. Phys. **B199**, 223 (1982).

[5] S. Dimopoulos, L. J. Hall, and S. Raby, Phys. Rev. Lett. **68**, 1984 (1992); Phys. Rev. D **45**, 4192 (1992); P. Ramond, Report No. UFIFT-92-4, 1992 (unpublished); H. Arason, D. Castano, E. J. Piard, and P. Ramond, Phys. Rev. D **47**, 232 (1993).

[6] G. Anderson, S. Raby, S. Dimopoulos, and L. J. Hall, Phys. Rev. D **47**, 3702 (1993); V. Barger, M. S. Berger, T. Han, and M. Zralek, Phys. Rev. Lett. **68**, 3394 (1992); V. Barger, M. S. Berger, and P. Ohmann, Phys. Rev. D **47**, 1093 (1993); **47**, 2038 (1993).

[7] H. Georgi, in *Particles and Fields—1974 (*APS/DPF *Williamsburgh),* Proceedings of the 1974 Meeting of the APS Division of Particles and Fields, edited by C. A. Carlson (AIP Conf. Proc. No. 23) (AIP, New York, 1975); H. Fritzsch and P. Minkovsky, Ann. Phys. **93**, 193 (1975).

[8] There are several symmetric textures with one less prediction: P. Ramond, R. G. Roberts, and G. G. Ross, Report No. RAL-93-010, 1993 (unpublished).

[9] S. Dimopoulos, Phys. Lett. **129B**, 417 (1983); J. Bagger, S. Dimopoulos, H. Georgi, and S. Raby, in *Proceedings of the Fifth Workshop on Grand Unification,* Providence, Rhode Island, 1984, edited by K. Kang, H. Fried, and P. Frampton (World Scientific, Singapore, 1984). See also the recent work of G. Lazarides and Q. Shafi, Nucl. Phys. **B350**, 179 (1991).

[10] C. D. Froggatt and H. B. Nielsen, Nucl. Phys. **B147**, 277 (1979).

[11] B. R. Greene, K. H. Kirklin, P. J. Miron, and G. G. Ross, Nucl. Phys. **B278**, 667 (1986).

[12] R. Barbieri, L. J. Hall, and S. Raby (unpublished).

[13] B. Ananthanarayan, G. Lazarides, and Q. Shafi, Phys. Rev. D **44**, 1613 (1991); H. Arason, D. Castano, B. Keszthelyi, S. Mikaelian, E. J. Piard, P. Ramond, and B. Wright, Phys. Rev. Lett. **67**, 2933 (1991).

[14] L. J. Hall, R. Rattazzi, and U. Sarid, LBL Report No. 33997, 1993 (unpublished).

[15] M. Olechowski and S. Pokorski, Phys. Lett. B **214**, 393 (1988); B. Ananthanarayan, G. Lazarides, and Q. Shafi (unpublished).

[16] L. J. Hall, R. Rattazzi, and U. Sarid (unpublished).

[17] R. Slansky, Phys. Rep. **79**, 1 (1981).

[18] R. N. Cahn, I. Hinchliffe, and L. J. Hall, Phys. Lett. **109B**, 426 (1982).

[19] F. del Aguila and L. E. Ibanez, Nucl. Phys. **B177**, 60 (1981).

[20] B. Grzadkowski, M. Lindner, and S. Theisen, Phys. Lett. B **198**, 64 (1987).

[21] C. Jarlskog, Phys. Rev. Lett. **55**, 1039 (1985).

[22] S. Sharpe, in *Lattice '91,* Proceedings of the International Symposium, Tsukuba, Japan, 1991, edited by M. Fukugita *et al.* [Nucl. Phys. B (Proc. Suppl.) **26**, 197 (1992)].

[23] D. Kaplan and A. Manohar, Phys. Rev. Lett. **56**, 2004 (1986).

[24] H. Leutwyler, Nucl. Phys. **B337**, 108 (1990).

[25] M. Olechowski and S. Pokorski, Phys. Lett. B **257**, 388 (1991).

[26] P. Drell and R. Patterson, in *Proceedings of the XXVIth International Conference on High Energy Physics,* Dallas, Texas, 1992, edited by J. Sanford, AIP Conf. Proc. No. 272 (AIP, New York, 1993), p. 3.

[27] J. M. Flynn, Mod. Phys. Lett. A **5**, 877 (1990); I. Dunietz, Ann. Phys. (N.Y.) **184**, 350 (1988).

[28] G. Buchalla, A. Buras, and M. Harlander, Nucl. Phys. **B337**, 313 (1990); A. Buras, M. Jamin, and M. Lautenbacher, Report No. MPI-Ph/93-11 (unpublished).

[29] Z. Kunszt and F. Zwirner, Nucl. Phys. **B385**, 3 (1992).

[30] L. J. Hall, in *Supersymmetry and Supergravity/ Nonperturbative QCD,* Proceedings of the Winter School in Theoretical Physics, Mahabaleshwar, India, 1984, edited by P. Roy and V. Singh, Lecture Notes in Physics Vol. 208 (Springer, Berlin, 1984).